Biological Journal of the Linnean Society, 2020, **129**, 950–974. With 16 figures.

Influence of mass on tarsus shape variation: a morphometrical investigation among Rhinocerotidae (Mammalia: Perissodactyla)

CYRIL ETIENNE[1,*], CHRISTOPHE MALLET[1], RAPHAËL CORNETTE[2] and ALEXANDRA HOUSSAYE[1]

[1]*UMR 7179, Mécanismes Adaptatifs et Evolution, Muséum National d'Histoire Naturelle, Centre National de la Recherche Scientifique, Paris, France*
[2]*UMR 7205, Institut de Systématique, Evolution, Biodiversité, Centre National de la Recherche Scientifique, Muséum National d'Histoire Naturelle, Sorbonne Université, Ecole Publique des Hautes Etudes, Paris, France*

Received 25 October 2019; revised 7 January 2020; accepted for publication 7 January 2020

Many tetrapod lineages show extreme increases in body mass in their evolutionary history, associated with important osteological changes. The ankle joint, essential for foot movement, is assumed to be particularly affected in this regard. We investigated the morphological adaptations of the astragalus and the calcaneus in Rhinocerotidae, and analysed them in light of a comparative analysis with other Perissodactyla. We performed 3D geometric morphometrics and correlated shape with centroid size of the bone and body mass of the species. Our results show that mass has an influence on bone shape in Rhinocerotidae and in Perissodactyla, but this is not as strong as expected. In heavy animals the astragalus has a flatter trochlea, orientated more proximally, associated with a more upright posture of the limb. The calcaneus is more robust, possibly to sustain the greater tension force exerted by the muscles during plantarflexion. Both bones show wider articular facets, providing greater cohesion and better dissipation of the loading forces. The body plan of the animals also has an influence. Short-legged Teleoceratina have a flatter astragalus than the other rhinocerotids. *Paraceratherium* has a thinner calcaneus than expected. This study clarifies adaptations to high body weight among Rhinocerotidae and calls for similar investigations in other groups with massive forms.

ADDITIONAL KEYWORDS: ankle – astragalus – calcaneus – functional morphology – high body weight – geometric morphometrics – Perissodactyla – Rhinocerotidae.

INTRODUCTION

In vertebrate locomotion, bone is a rigid organ of paramount importance. It provides support for the body as well as attachment points for the muscles, via the tendons (Hildebrand, 1982; Biewener, 1990). Bone shape varies with a diversity of factors, one of the main ones being the size of the animal (Hildebrand *et al.*, 1985; Biewener, 1989; Polly, 2008; Biewener & Patek, 2018). Evolutionary convergences are usually observed when similar selective pressures are applied to the same structure independently in different groups. Accordingly, in a given clade, an increasing body mass generally results in, for example, a more vertical orientation of the pelvis (Polly, 2008), an increasing diameter of the femur (Alexander, 1985) and micro-anatomical changes such as a thick cortical bone (Houssaye *et al.*, 2016). Postural and locomotor factors such as facultative bipedalism or cursoriality are also important factors influencing the shape of the skeleton (Hildebrand, 1982; Polly, 2008). Analysing the relationship between mass and the shape of the bones, while also considering factors such as posture and locomotion, would allow a better understanding of the way animals with different body plans adapt to an increasing mass.

Rhinocerotidae (Gray, 1821) seem to be an excellent group to study morphological variations in bone related to mass and to a varying body plan. Today

*Corresponding author. E-mail: cyril.etienne@cri-paris.org

comprising five species and four genera, rhinocerotids are found only in tropical regions (Dinerstein, 2011). They were much more diverse during the Cenozoic, appearing in the mid-Eocene and comprising more than 100 species (Cerdeño, 1998). Rhinocerotids have been found in Eurasia, Africa and North America (as far south as Panama; MacFadden, 2006), and existed in a diversity of habitats, such as cold steppes, dense forests and swamps (Prothero *et al.*, 1989; Mörs, 2002; Prothero, 2005). All of them were relatively heavy animals as compared to the average body mass of mammals (Gardezi & da Silva, 1999), ranging from ~150 kg for the lightest taxa of the Eocene to 5 tons for *Elasmotherium* (Cerdeño, 1998; Becker, 2003; Antoine, 2020). They have undergone several independent extreme increases in body mass, up to more than 2 tons, during their evolutionary history (e.g. in Rhinocerotina, Teleoceratina or Elasmotheriinae; Cerdeño, 1998). They also vary in terms of body plan: some taxa are massive and sturdy (e.g. *Coelodonta*, *Ceratotherium*), some are extremely short-legged (e.g. *Teleoceras*, *Brachypotherium*, *Prosantorhinus* in the Teleoceratina tribe), while others have been described as gracile and cursorial (e.g. *Protaceratherium*, *Hispanotherium*; Cerdeño, 1998). Rhinocerotids should therefore be a very interesting group to study variations in bone shape, and analyse its relationship with different masses and morphologies. Rhinocerotidae are part of the order Perissodactyla (Owen, 1848). The Perissodactyla today only include the five species of Rhinocerotidae, the seven species of Equidae and the four species of Tapiridae, but were far more diversified during the Cenozoic, in terms of number of both species and families (Prothero & Schoch, 1989; Fig 1). They included notably the Paraceratheriidae (sometimes considered a subfamily of Hyracodontidae, see Wang *et al.*, 2016), which included some of the heaviest land mammals that have ever lived (Prothero, 2013). Perissodactyla also included the intriguing Chalicotheriidae, among which some species (the subfamily Chalicotheriinae) were facultative bipeds with a gorilla-like stance, with very short hindlimbs, and walked on the knuckles of their forelimbs, whereas others (the Schizotheriinae) had front and hindlimbs of approximately equal length (Coombs, 1983; Semprebon *et al.*, 2011). This order therefore encompasses a great diversity in terms of mass and body plan that can be related to their bone shape, and as compared with the diversity observed among Rhinocerotidae.

Our study focuses on two bones of the tarsus: the astragalus and the calcaneus. These bones are at the junction between the hind zeugopodium and the autopodium, and are essential to the movement of the foot and consequently of the entire animal. The astragalus serves as the pivot, or fulcrum, and the calcaneus as the lever arm of the foot (Carrano, 1997). These bones have been extensively studied, from taxonomic and phylogenetic points of view (see Stains, 1959; Guérin, 1980; Missiaen *et al.*, 2006; Gladman *et al.*, 2013), but also in a morphofunctional context, with multiple studies trying to link their shape to the animal's mass (see Dagosto & Terranova, 1992; Martinez & Sudre, 1995; Tsubamoto, 2014), habitat (DeGusta & Vrba, 2003; Plummer *et al.*, 2008; Curran, 2012; Barr, 2014) and mode of locomotion (Nakatsukasa *et al.*, 1997; Panciroli *et al.*, 2017). These studies all found a link between the mass of a species and the shape both of its astragalus and of its calcaneus, generally represented by linear measurements or ratios. These studies concerned a wide variety of mammals (e.g. bovids, cervids, carnivorans and primates), but none specifically studied the relationship between mass and shape on both ankle bones in perissodactyls.

In the present study, we investigated the variation of the shape of the astragalus and calcaneus across a diversity of extant and fossil Rhinocerotidae and additional Perissodactyla. Our primary aim was to identify shape variations associated with an increase of mass. We expect that mass will have a strong influence on those bones because they are extremely important for support and movement in mammals. We expect that bones of large animals will be more robust and more resistant, with wider and flatter articular facets to help dissipate forces. We also expect that adaptations will vary according to the general body plan and mode of locomotion of the animal. We studied variations of bone shape, and tested the influence of bone size and of the mean mass of each species. We first focused on shape variations across Rhinocerotidae, and then across all Perissodactyla sampled in order to compare the variations observed among Rhinocerotidae to more diverse forms (e.g. *Paraceratherium*), and thus better interpret the drivers acting on this variation.

MATERIAL AND METHODS

Material

We studied 112 astragali and 94 calcanei belonging to 43 different species across five different families of Perissodactyla, with varying masses, morphologies or locomotor modes (Supporting Information, Appendix S1; Fig. 1). Taxa were chosen to encompass as much as possible of the variation within Rhinocerotidae. A few specimens of other families of Perissodactyla with particular characteristics (e.g. an extremely high mass for *Paraceratherium*, cursoriality for horses, shortened hindlimbs for Chalicotheriinae) were included to provide a comparison point for the shape variations observed in Rhinocerotidae. Rhinocerotidae constitute our main subsample, with 40 specimens of each bone type for living

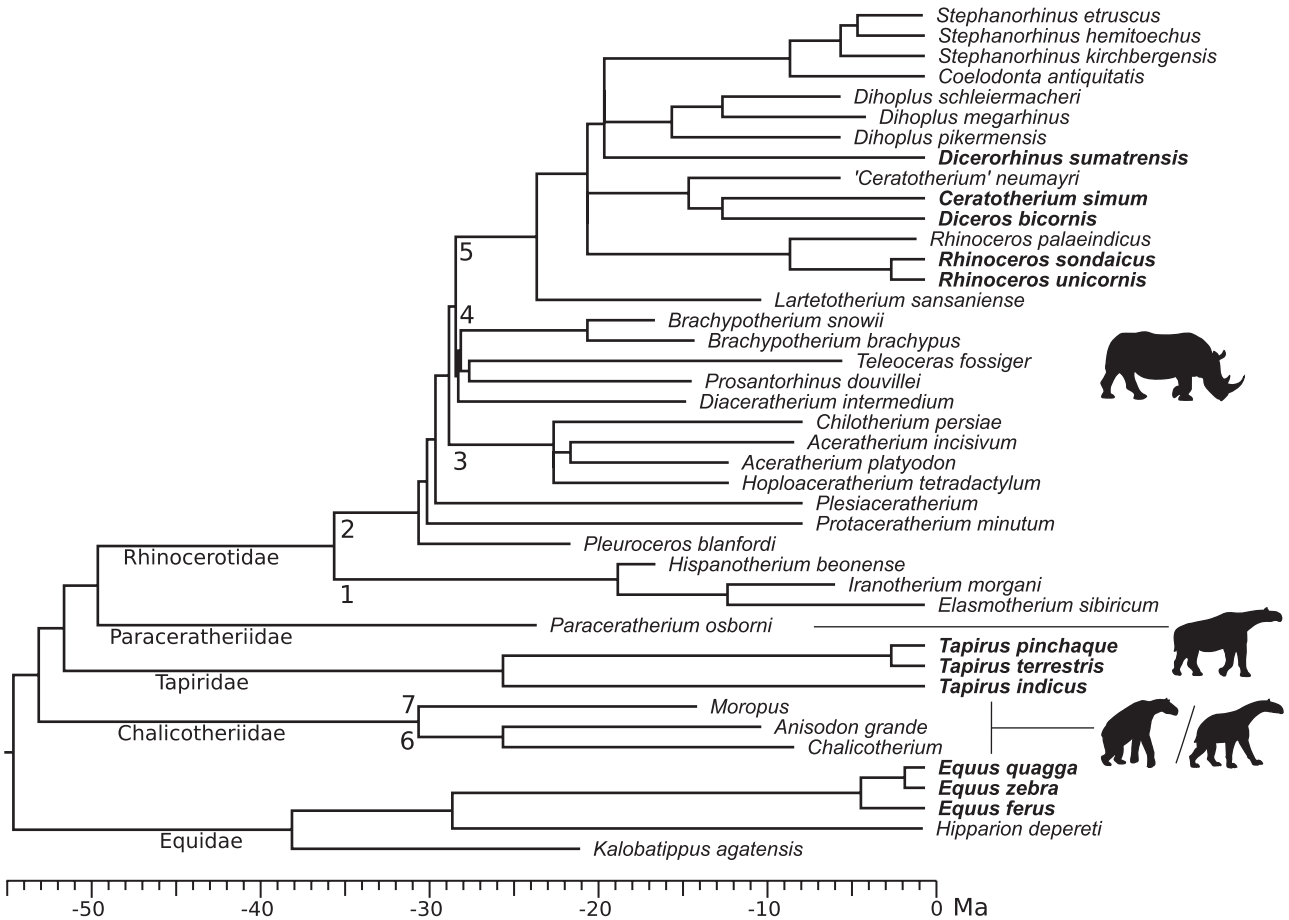

Figure 1. Composite phylogeny including the species sampled (modified from Antoine, 2002; Antoine *et al.*, 2010, 2020; Piras *et al.*, 2010; Holbrook & Lapergola, 2011; Steiner and Ryder, 2011). Occurrence dates were estimated from Antoine (1997), Piras *et al.* (2010), Antoine *et al.* (2010), Geraads *et al.* (2012), Guérin (2012) and Prothero (2013), as well as data recorded on http://fossilworks.org. 1, Elasmotheriinae; 2, Rhinocerotinae; 3, Aceratheriina; 4, Teleoceratina; 5, Rhinocerotina; 6, Schizotheriinae; 7, Chalicotheriinae. Species in bold are extant. The relationships between the five extant rhino species remain in debate; specifically the position of *Dicerorhinus sumatrensis* and its close fossil relatives is uncertain, placed either as sister taxa to *Ceratotherium* and *Diceros*, as sister taxa to *Rhinoceros*, or as sister taxa to a group comprising *Rhinoceros*, *Ceratotherium* and *Diceros* (Willerslev *et al.*, 2009; Gaudry, 2017). This phylogenetic uncertainty is here represented by a polytomy.

species. Our sample also includes 43 astragali and 31 calcanei of fossil Rhinocerotidae, including small, cursorial genera (*Protaceratherium*, *Pleuroceros*), and at least three lineages showing independent increases in body mass above 2 tons (in *Elasmotherium*, *Brachypotherium* and *Coelodonta*, plus the living *Ceratotherium* and *Rhinoceros unicornis*). We studied ten astragali and calcanei of extant Tapiridae, and eight astragali and six calcanei of Equidae. Three astragali and one calcaneus belong to *Paraceratherium* (Paraceratheriidae), and eight astragali and six calcanei belong to Chalicotheriidae. To our knowledge, all the bones belonged to adult specimens. A description of the bones, including the nomenclature used for the main anatomical features of the bones, is provided in Appendix S2.

Specimens come from the collections of the Muséum National d'Histoire Naturelle (MNHN, Paris, France), the Muséum d'Histoire Naturelle de Toulouse (MHNT, Toulouse, France), the Claude Bernard University (UCBL, Lyon, France), the Natural History Museum (NHM, London, UK), the Powell-Cotton Museum (BICPC, Birchington-on-Sea, UK), the Naturhistorisches Museum Wien (NMW, Vienna, Austria), the Zoologische Staatssammlung München (ZSM, Munich, Germany) and the Bayerische Staatssammlung für Paläontologie und Historiche Geologie (BSPHM, Munich, Germany; Supporting information, Appendix S1).

Mass estimations used

Mass data were retrieved from the literature (Table 1). Methods of mass reconstructions are detailed in the references; they usually relied on regression equations and measurements on the molars or on proximal limb segments. None of them used measurements on the

Table 1. List of the masses used for the species studied here

Family	Species	Mass (kg)	Source
Rhinocerotidae	*Rhinoceros sondaicus*	1200–1500	Dinerstein (2011)
Rhinocerotidae	*Rhinoceros unicornis*	2000	Dinerstein (2011)
Rhinocerotidae	*Rhinoceros palaeindicus* †	Missing data	
Rhinocerotidae	*Diceros bicornis*	800–1300	Dinerstein (2011)
Rhinocerotidae	*Ceratotherium neumayri* †	1200	Valli (2005)
Rhinocerotidae	*Ceratotherium simum*	2300	Dinerstein (2011)
Rhinocerotidae	*Dicerorhinus sumatrensis*	600–950	Dinerstein (2011)
Rhinocerotidae	*Stephanorhinus etruscus* †	Missing data	
Rhinocerotidae	*Stephanorhinus kirchbergensis* †	1844	Saarinen *et al.* (2016)
Rhinocerotidae	*Stephanorhinus hemitoechus* †	Missing data	
Rhinocerotidae	*Coelodonta antiquitatis* †	1905	Saarinen *et al.* (2016)
Rhinocerotidae	*Dihoplus megarhinus* †	Missing data	
Rhinocerotidae	*Dihoplus schleiermacheri* †	1812	Becker (2003)
Rhinocerotidae	*Dihoplus pikermensis* †	1100	Valli (2005)
Rhinocerotidae	*Lartetotherium sansaniense* †	1204	Becker (2003)
Rhinocerotidae	*Prosantorhinus douvillei* †	Missing data	
Rhinocerotidae	*Teleoceras fossiger* †	1016	Damuth (1990)
Rhinocerotidae	*Brachypotherium brachypus* †	2327	Becker (2003)
Rhinocerotidae	*Brachypotherium snowi* †	Missing data	
Rhinocerotidae	*Aceratherium incisivum* †	1982	Becker (2003)
Rhinocerotidae	*Aceratherium platyodon* †	Missing data	
Rhinocerotidae	*Hoploaceratherium tetradactylum* †	1197	Becker (2003)
Rhinocerotidae	*Chilotherium persiae* †	Missing data	
Rhinocerotidae	*Diaceratherium intermedium* †	Missing data	
Rhinocerotidae	*Plesiaceratherium* †	Missing data	
Rhinocerotidae	*Protaceratherium minutum* †	530	Becker (2003)
Rhinocerotidae	*Pleuroceros blanfordi* †	501	Becker (2003)
Rhinocerotidae	*Victoriaceros kenyensis* †	Missing data	
Rhinocerotidae	*Hispanotherium beonense* †	Missing data	
Rhinocerotidae	*Elasmotherium sibiricum* †	4000–5000	Zhegallo *et al.* (2005)
Rhinocerotidae	*Iranotherium morgani* †	Missing data	
Paraceratheriidae †	*Paraceratherium bugtiense* †	7400	Fortelius & Kappelman (1993)
Tapiridae	*Tapirus pinchaque*	150–200	Medici (2011)
Tapiridae	*Tapirus terrestris*	220	Medici (2011)
Tapiridae	*Tapirus indicus*	280–400	Medici (2011)
Chalicotheriidae †	*Chalicotherium sp.* †	924	Costeur (2004)
Chalicotheriidae †	*Anisodon grande* †	1500	Guérin (2012)
Chalicotheriidae †	*Moropus sp.* †	1179	Damuth (1990)
Equidae	*Equus zebra*	240–380	Rubenstein (2011)
Equidae	*Equus quagga*	175–320	Rubenstein (2011)
Equidae	*Equus przewalski*	200–300	Rubenstein (2011)
Equidae	*Equus caballus*	380–600	Bongianni (1988)
Equidae	*Equus caballus* *	700–1000	Bongianni (1988)
Equidae	*Hipparion depereti* †	Missing data	
Equidae	*Kalobatippus agatensis* †	160	Jams *et al.* (1994)

†Fossil taxon.
*Two separate mass estimates were used for *Equus caballus*, one for average-sized horses and one for draught horses, given the wide morphological differences between the two.

astragalus or the calcaneus. When only a range of masses was available with no average, the mean of the minimal and maximal mass was used.

Data acquisition

The specimens were digitized using either an Artec Eva surface scanner and the Artec Studio Professional v.12.1.5.1 software (Artec 3D, 2018), or a Nikon D5500 camera (automatic mode, without flash, focal length 50 mm, aperture f/1.8) and the photogrammetry software Agisoft PhotoScan v.1.4.0 (Agisoft LLC, 2017). The 3D meshes were then exported, reduced to 60 000 faces and mirrored to have only right-side astragali and calcanei, using MeshLab v.2016.12 (Cignoni *et al.*, 2008). In two cases (astragalus of *Brachypotherium snowi* NHM-PAL-PV-M-29279 and calcaneus of *Hispanotherium beonense* MHNT-2015-0-837), the specimens were slightly damaged were curve semi-landmarks would be placed and had to be partially reconstructed using Geomagic (3D Systems, 2017).

Geometric morphometrics

Bone shape was modelled using anatomical landmarks and semi-landmarks sliding on curves (Gunz & Mitteroecker, 2013). Landmarks were all placed by the same operator (C.E.). Given that there can be marked differences in bone shape between rhinocerotids and the other perissodactyls, we split the analysis in two. Two sets of landmarks and curves were therefore defined: one for all the rhinocerotids, and another for all the perissodactyls (see Figs 2, 3; Supporting Information, Appendix S3 for descriptions of the landmarks and curves), with fewer landmarks and curves but able to encompass a broader number of taxa. The second set is mostly a subset of the first one,

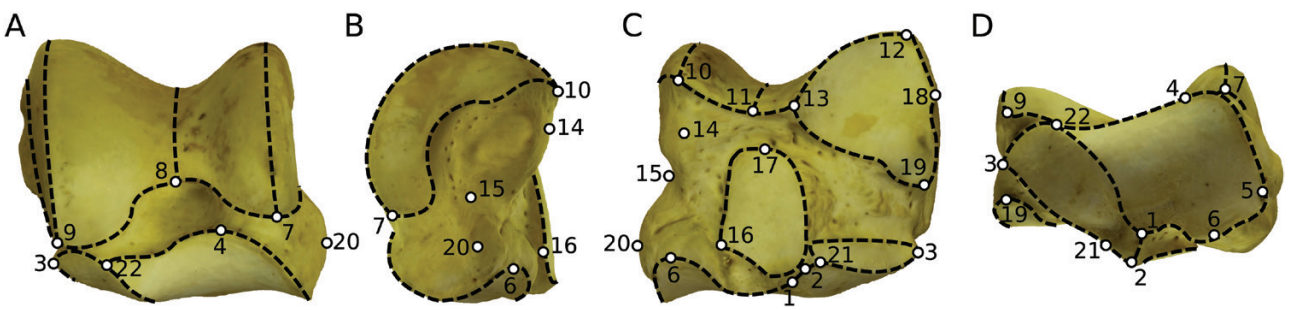

Figure 2. Representation of the landmarks and the curves placed on the astragalus of *Rhinoceros unicornis* MNHN-ZM-AC-1960-59. A, anterior; B, medial; C, posterior; and D, distal views. White dots denote the 22 anatomical landmarks, and dotted black lines the nine curves. Descriptions of the landmarks and curves are provided in Appendix S3.

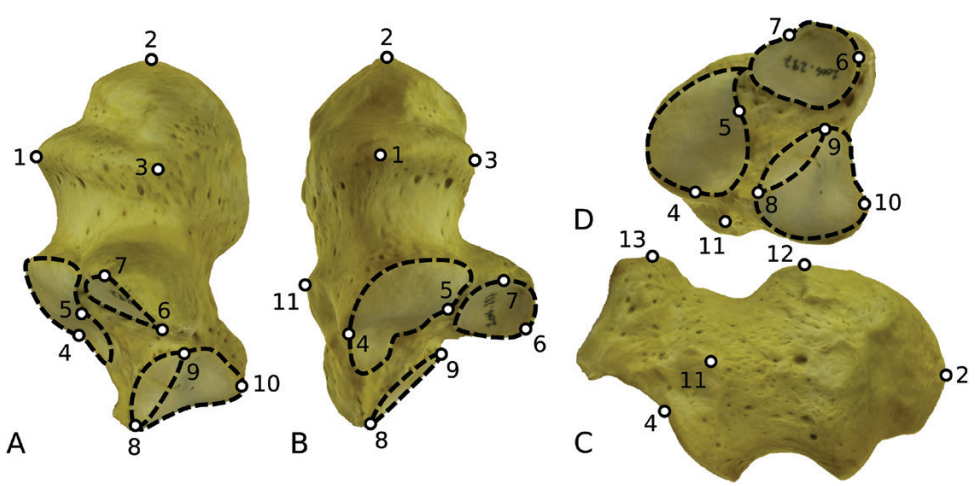

Figure 3. Representation of the landmarks and curves placed on the calcaneus of *Ceratotherium simum* MNHN-ZM-MO-2005–297. A, medial; B, anterior; C, latero-anterior; and D, distal views. White dots denote the 13 anatomical landmarks, and dotted black lines the four curves. Descriptions of the landmarks and curves are provided in Appendix S3.

so only two curves had to be redefined. Landmarks and curves were digitized on the meshes using the IDAV Landmark software package (Wiley, 2005). All the analyses and statistical tests were run using R (R Development Core Team, 2005) and RStudio (RStudio, Inc., 2018). The curves were resampled using the algorithm provided by Botton-Divet *et al.* (2016). Then, as the algorithm can result in some semi-landmarks being slightly above or below the mesh surface, the semi-landmarks were reprojected on the meshes using the closemeshKD function of the Morpho R package (Schlager *et al.*, 2018), which uses the coordinates of each semi-landmark to calculate its closest match on the surface of the mesh.

Landmarks were superimposed using a Generalized Procrustes Analysis (GPA), which translates, scales and rotates each set of landmarks to remove the information on size, position and angle, and to minimize the sum of square distances between landmark configurations (Bookstein, 1991). The curve semi-landmarks were slid along the curves to minimize the bending energy of a thin-plate-spline as described by Gunz *et al.* (2005). The bending energy is a scalar quantity that roughly represents the amount of local shape deformation between a reference set of landmarks (chosen arbitrarily among our sample). More technically, it is the integral of the squared second derivatives of the deformation (see Mitteroecker & Gunz, 2009; Gunz & Mitteroecker, 2013).

To assess the repeatability of the landmarks, and before placing the landmarks on the whole sample, we placed each landmark ten times on each of three specimens of *Diceros bicornis*, alternating between each specimen. The three specimens were assessed by sight to be the three morphologically closest. These 30 landmark sets were then superimposed using a GPA and visualized using a principal components analysis (PCA), to check that landmark error per specimen was smaller than inter-individual variation (Supporting Information, Appendix S4).

Statistical analyses

After the GPA, the aligned landmark coordinates were used in a PCA to reduce the dimensionality of our data and assess the shape variation patterns in our sample. Neighbour-joining trees were generated using a Euclidian distance matrix based on the PC-scores, in order to visualize the phenotypic similarities between each specimen or group in a multivariate manner, instead of one axis at a time, which is useful if each axis explains a small percentage of the variance. PC-scores were used instead of Procrustes coordinates to reduce the number of dimensions and thus lower the computing power required.

We tested the influence of the centroid size of each bone on its shape. Centroid size is defined as the square root of the sum of the square of the distance of each point to the centroid of the landmark set; it is most commonly used to assess the variations of shape that are due to variations of size, or allometry (Mitteroecker *et al.*, 2013; Klingenberg, 2016). Logarithms were used for the centroid size values, as recommended by Bookstein (1991) and Klingenberg (1996). Procrustes coordinates were correlated against centroid size using a multivariate regression. The allometry-free residuals from the tests were used to create allometry-free shapes for each individual, allowing analyses in which the influence of size is entirely removed (e.g. Evin *et al.*, 2011; Perrard *et al.*, 2012).

The centroid size of both bones is statistically linked to the mean mass of the species in our sample (see Supporting Information, Appendix S5; $P < 0.0001$, R^2 between 0.46 and 0.82 depending on the bone and the landmark set). The R^2 value is, however, different from 1, and therefore mass could have an influence on the shape of the bones that is independent of its centroid size. For example, two astragali or calcanei with the same centroid size belonging to species with different mean masses would exhibit divergent shapes. This was tested using a multivariate regression of the allometry-free shapes generated earlier on the logarithm of the cubic root of the mean mass of the species. Given that we could not find mass estimation for 14 sampled species, they have been removed from this analysis.

To assess the effect of shared evolutionary history of different species on the shape of the astragalus and calcaneus, the degree of phylogenetic signal in the morphological data was also assessed, using a multivariate K statistic (K-mult) based on the PC-scores. This compares the observed rate of morphological change to the expected change under Brownian motion (see Blomberg *et al.*, 2003; Adams, 2014). The phylogeny used is provided in Figure 1. The results are provided in Supporting Information, Appendix S6.

Thin plate splines were used to visualize the results of our analyses: for each set of landmarks on the calcaneus and astragalus, the mean shape generated by the GPA was mapped onto the specimen closest to the mean value. This mean-shaped model was then deformed towards the shape resulting from our analyses, for instance the shape extremes of each PCA axis.

RESULTS

Rhinocerotidae

Astragalus

Morphological variations: The neighbour-joining tree (Fig. 4) generally shows a greater morphological

proximity between members of the same species than between members of different species, which indicates that interspecific variation is generally greater than intraspecific variation. The Teleoceratina, the short-legged rhinocerotids, are clearly grouped and separated from the others, except *Diaceratherium*. Among them, *Teleoceras* has a very long branch indicating a very derived morphology for this individual. *Dicerorhinus*, *Ceratotherium simum* and *Rhinoceros* all form homogeneous groups, but *Diceros* has two specimens that are separated from the others. This might be due to them possibly either belonging to different subspecies or a different sex, but this is unknown for these specimens. All the fossil dicerorhinins (*Dihoplus*, *Stephanorhinus* and *Coelodonta*) are grouped together, but *Dicerorhinus sumatrensis* is separated from them. Aceratheriina, Elasmotheriinae, *Diaceratherium*, *Protaceratherium*, *Pleuroceros* and *Plesiaceratherium* tend to all group together, with a few exceptions. The two specimens of *Iranotherium morgani* are clearly separated from one another in the tree; this is also the case for the two *Ceratotherium neumayri* specimens. Above the tribe level, there are no clusters that seem to follow the phylogeny.

A low percentage of variance is explained by each axis of the PCA on Rhinocerotidae astragali (63.1% for the first ten axes). Only the principal components that are correlated to centroid size, or that highlight variations of shape that could be due to differences in terms of animal general body plan, are described. Thus, only PC1, PC2 and PC4 are described here. PC1 highlights differences in astragalus shape between species with different morphologies, and PC2 and PC4 are weakly but significantly correlated with centroid size. PC2 is positively correlated with centroid size ($P < 0.001$, $R^2 = 0.17$), and PC4 is negatively correlated with centroid size ($P < 0.001$, $R^2 = 0.12$). Vector representations of the deformations along the principal components are provided in Supporting Information, Appendix S7.

PC1 (14.2% of the variance, Fig. 5) strongly separates members of the short-legged Teleoceratina, on the negative side, from the other Rhinocerotidae. The axis is characterized in its negative extremity by large proximo-distal compression of the bone; a flatter and symmetrical trochlea with medio-laterally wider and lower ridges; and a trochlea with a more proximal than anterior orientation. Regarding the articular facets, at the negative side of PC1 the proximal facet with the calcaneus is distally elongate; the medial facet for the calcaneus is proximo-distally compressed, twice as broad (medio-laterally) as high (proximo-distally), and not fused to the distal facet; the distal facet for the calcaneus is medio-laterally very short; and the facet for the navicular is broader than on the positive extremity of the axis, covering most of the distal face of the astragalus.

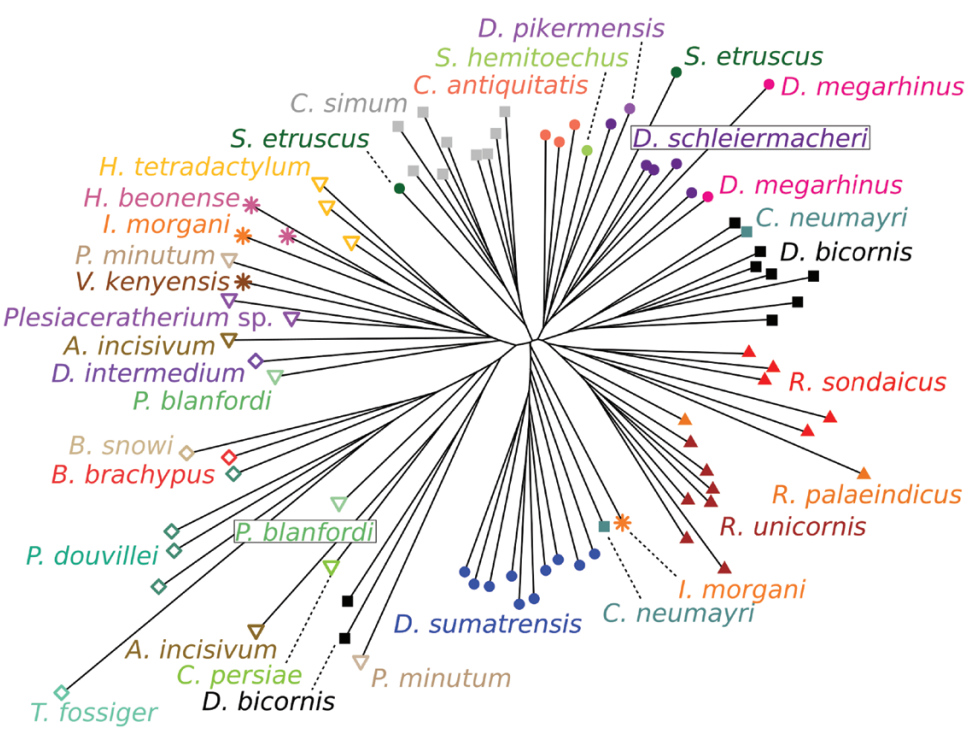

Figure 4. Neighbour-joining tree generated from a matrix of the Euclidian distance between every specimen, on the astragali of Rhinocerotidae. Legend as in Figure 5.

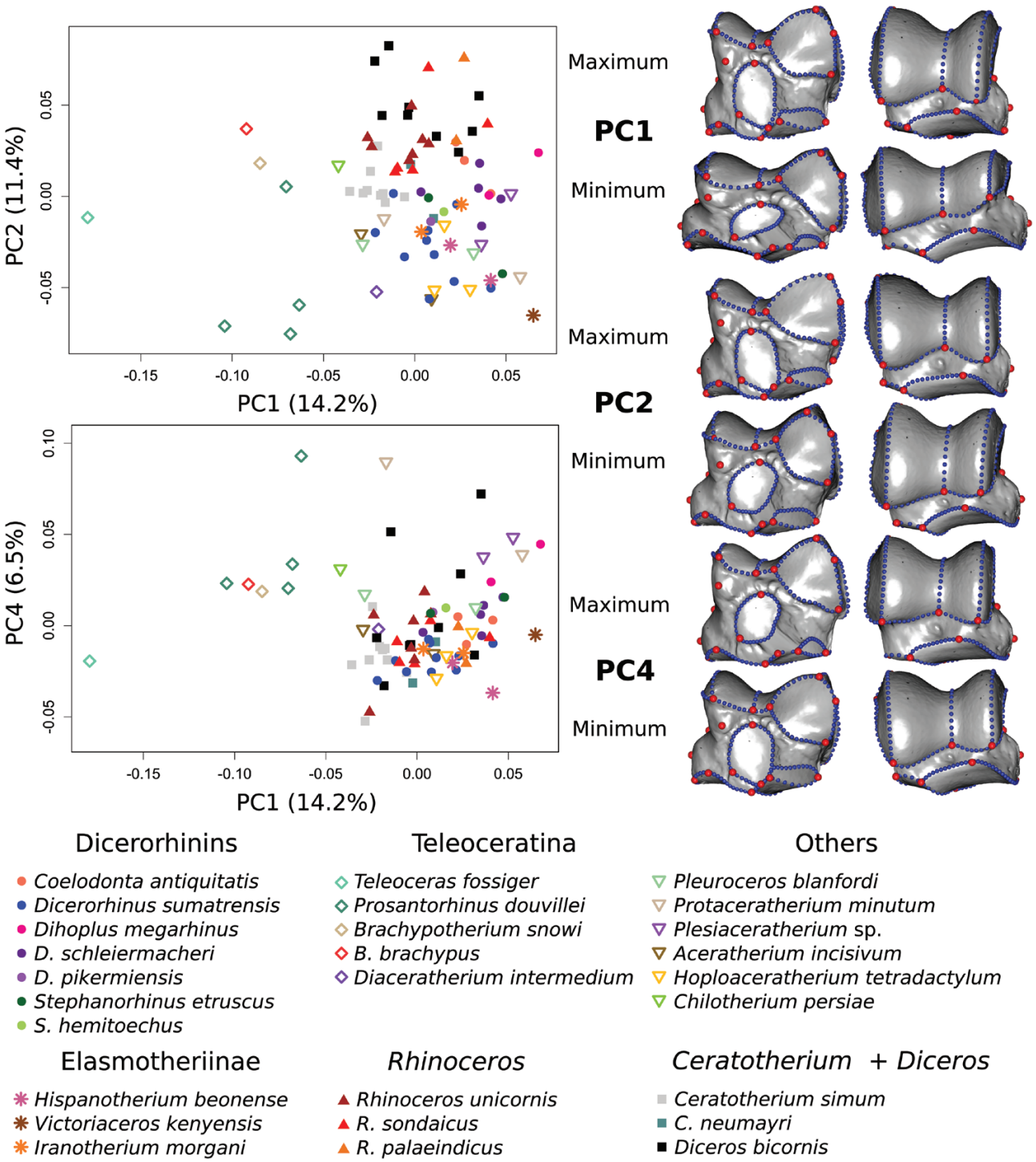

Figure 5. Results of the PCA performed on the astragalus of Rhinocerotidae. Left: repartition of the Rhinocerotidae astragali studied across PC1, PC2 and PC4. Right: thin-plate-spline deformation of a mean shape towards the maximal and minimal value of each axis. The view is first posterior then anterior. Red dots denote landmarks and blue dots denote curve semi-landmarks. Vector representations of the deformations are provided in Appendix S7A.

Along PC2 (11.4% of the variance, Fig. 5), *Diceros*, *Rhinoceros* and *Brachypotherium* are placed on the positive side, and *Dicerorhinus*, *Hoploaceratherium*, *Aceratherium*, *Hispanotherium* and *Victoriaceros* on the negative side, the other genera being scattered around the centre. Teleoceratina are spread across the

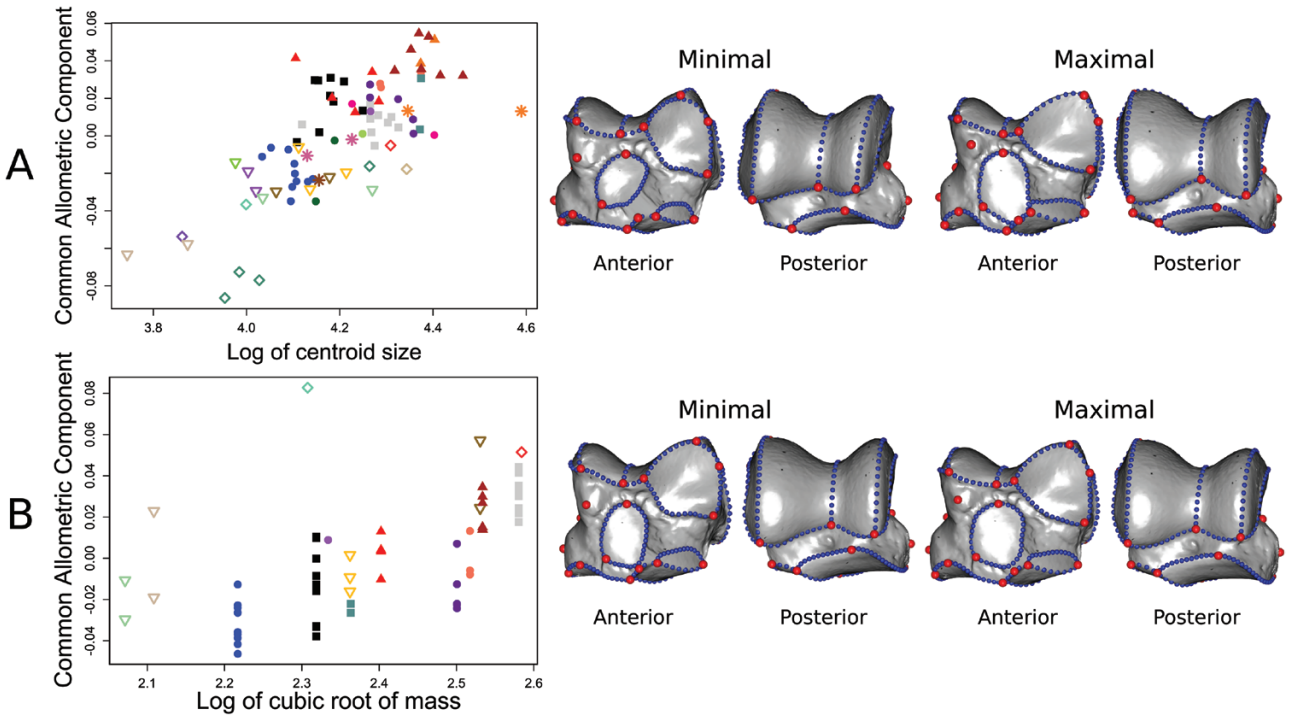

Figure 6. A, regression of the common allometric component on the logarithm of centroid size, with representations of the shapes corresponding to the theoretical maximum and minimum of allometry, on Rhinocerotidae astragali. B, regression of the common allometric component of allometry-free shapes, on the logarithm of the cubic root of the mean mass of the species, with representations of the shapes corresponding to the theoretical maximum and minimum of mass, on Rhinocerotidae astragali. Legend as in Figure 5. Vector representations are available in Appendix S7B.

whole axis. The axis is characterized at its negative extremity by a higher lateral ridge of the trochlea than observed on the positive side; a less concave distal contour of the trochlea; the pentagonal shape of the proximal facet for the calcaneus, in contrast to the medio-laterally wider triangular shape observed on the positive side; and a proximo-distal shortening of the medial facet for the calcaneus, which does not reach the distalmost point of the bone as it does on the positive side.

PC4 (6.5% of the variance, Fig. 5) shows *Protaceratherium*, *Plesiaceratherium* and *Prosantorhinus* on the positive part of the axis, and *Hispanotherium*, *Iranotherium*, *Hoploaceratherium*, *Ceratotherium*, *Dicerorhinus* and *Teleoceras* on the negative part. It is characterized at its negative extremity by a very short neck of the astragalus; a more proximal orientation of the trochlea; a distal shortening of the proximal facet for the calcaneus; and a fusion of the medial and distal facets for the calcaneus, whereas both are very well separated on the positive part of the axis.

Impact of allometry and mass: Centroid size has a significant but weak effect on the shape of the astragalus ($P < 0.01$, $R^2 = 0.04$, according to multivariate regression of the logarithm of centroid size on the Procrustes coordinates). A large astragalus (Fig. 6A) is characterized by a medio-laterally wider and triangle-shaped proximal facet with the calcaneus; medio-laterally wider and fused medial and distal facets with the calcaneus; and an articular facet with the navicular positioned less laterally offset, more directly underneath the rest of the bone.

Once the influence of centroid size is removed, there is only a weak influence of the mass of the species on the shape of the astragalus ($P < 0.05$, $R^2 = 0.03$). The shape variations are minimal: in an astragalus pertaining to a heavy species (Fig. 6B), the facets for both malleoli are enlarged, the crescent they form being wider; the proximal facet for the calcaneus is slightly more triangle-shaped; the medial facet is slightly wider medio-laterally; and the facet for the cuboid and the distal facet for the calcaneus are anteriorly extended.

Calcaneus

Morphological variations: The neighbour-joining tree based on calcaneal morphology (Fig. 7) indicates, as for the astragalus, a tendency for individuals of the

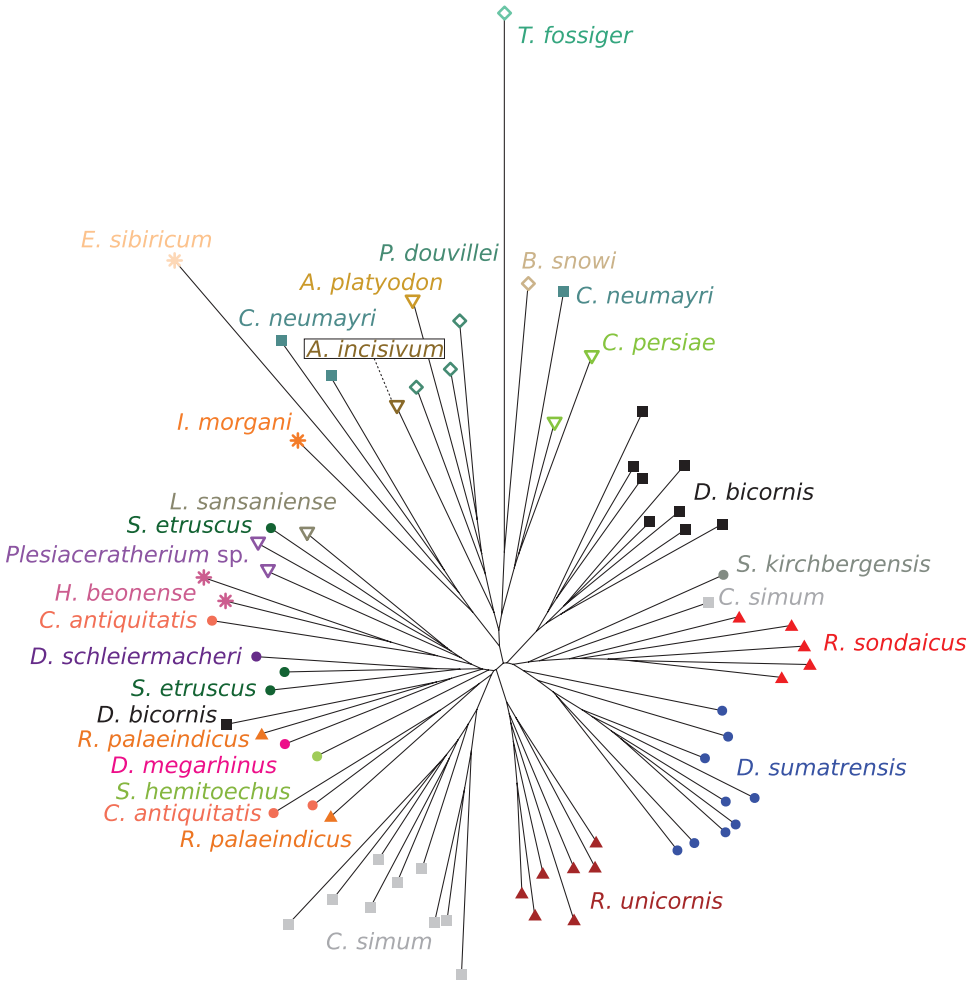

Figure 7. Neighbour-joining tree generated from a matrix of the Euclidian distance between every specimen, on the calcanei of Rhinocerotidae. Legend as in Figure 8.

same species to be grouped together. Teleoceratina are grouped with Aceratheriina, and *Teleoceras fossiger* has again the longest branch of all species. *Elasmotherium sibiricum* has also a particularly long branch. There seem to be fewer clusters of species belonging to the same higher-rank taxon than for the astragalus. Notably, the three species of the genus *Rhinoceros*, notably are scattered in the tree. *Ceratotherium neumayri* is close to *Chilotherium* and *Elasmotherium sibiricum*, and most extinct dicerorhinins are grouped with *Rhinoceros palaeindicus*, *Hispanotherium beonense* and *Plesiaceratherium*. Again, for taxa of higher rank than tribes, there are no clusters that follow the phylogeny.

As for the astragalus, a low percentage of variance is explained by each axis (66.3% for the first ten axes). Only the first two axes are described, as the first one is linked to centroid size and the second one to variations in the body plan of rhinoceroses. PC1 is weakly and negatively correlated with centroid size ($P < 0.01$, $R^2 = 0.11$).

PC1 (12.4% of the variance, Fig. 8) shows *Elasmotherium* as the genus with the most negative value, along with *Ceratotherium*, *Iranotherium* and *Lartetotherium*. *Diceros* has slightly negative values and *Rhinoceros* slightly positive values. *Dicerorhinus*, *Teleoceras* and *Brachypotherium* have the most positive values on this axis. The axis is characterized at its negative extremity by a more robust tuber calcanei; a proximal facet for the astragalus that is medio-laterally wider in its proximal half, and distally extended; a longer distal facet for the astragalus; and a larger, proximally extended facet for the cuboid whereas it is piriform (proximally reduced and distally extended) on the positive part of the axis.

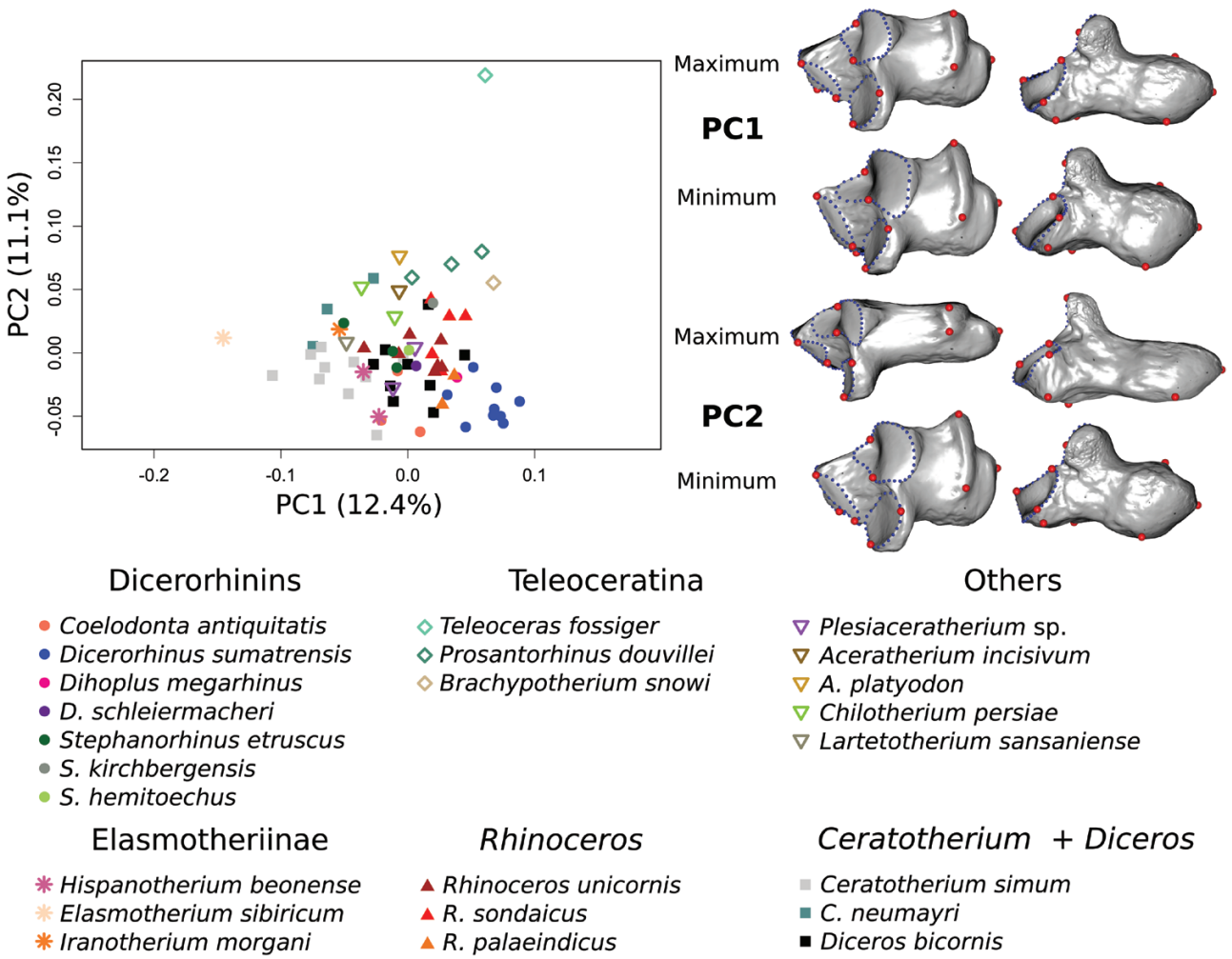

Figure 8. Results of the PCA performed on the calcanei of Rhinocerotidae. Left: repartition of the Rhinocerotidae calcanei studied across the first two PCA axes. Right: thin-plate-spline deformation of a mean shape towards the maximal and minimal values of each axis. The view is first antero-medial then postero-medial. Red dots denote landmarks and blue dots denote curve semi-landmarks. Vector representations of the deformations are provided in Appendix S7C.

PC2 (11.1%, Fig. 8) separates strongly our *Teleoceras* specimen on the negative part from the other genera. The other Teleoceratina, *Chilotherium* and *Aceratherium*, have, among the other genera, the most positive values and thus are the closest to *Teleoceras*. PC2 is characterized at its positive extremity by a more gracile tuber calcanei; a reduction of the medio-lateral width of the proximal part of the proximal facet for the astragalus; a medio-laterally wider and distally longer distal part of the proximal facet for the astragalus than on the negative extremity of the axis; a proximo-distally compressed medial facet for the astragalus (twice as wide as it is high); a much less elongated distal facet for the astragalus; and an antero-posteriorly compressed facet for the cuboid.

Impact of allometry and mass: Centroid size has a significant but weak effect on the shape of the calcaneus ($P < 0.01$, $R^2 = 0.04$; multivariate regression). A large calcaneus (Fig. 9A) has a medio-laterally wider proximal part of the proximal facet for the astragalus; a wider medial facet for the astragalus, expanding distally and merging with the distal facet for the astragalus; an elongated distal facet for the astragalus; and a sustentaculum tali orientated more distally, whereas it is orientated antero-distally in small calcanei.

Mass has a slightly stronger influence on the allometry-free shapes of the calcaneus than on those of the astragalus ($P < 0.001$, $R^2 = 0.06$). A calcaneus belonging to a heavy species (Fig. 9B) has a more robust tuber calcanei than a calcaneus belonging to a light

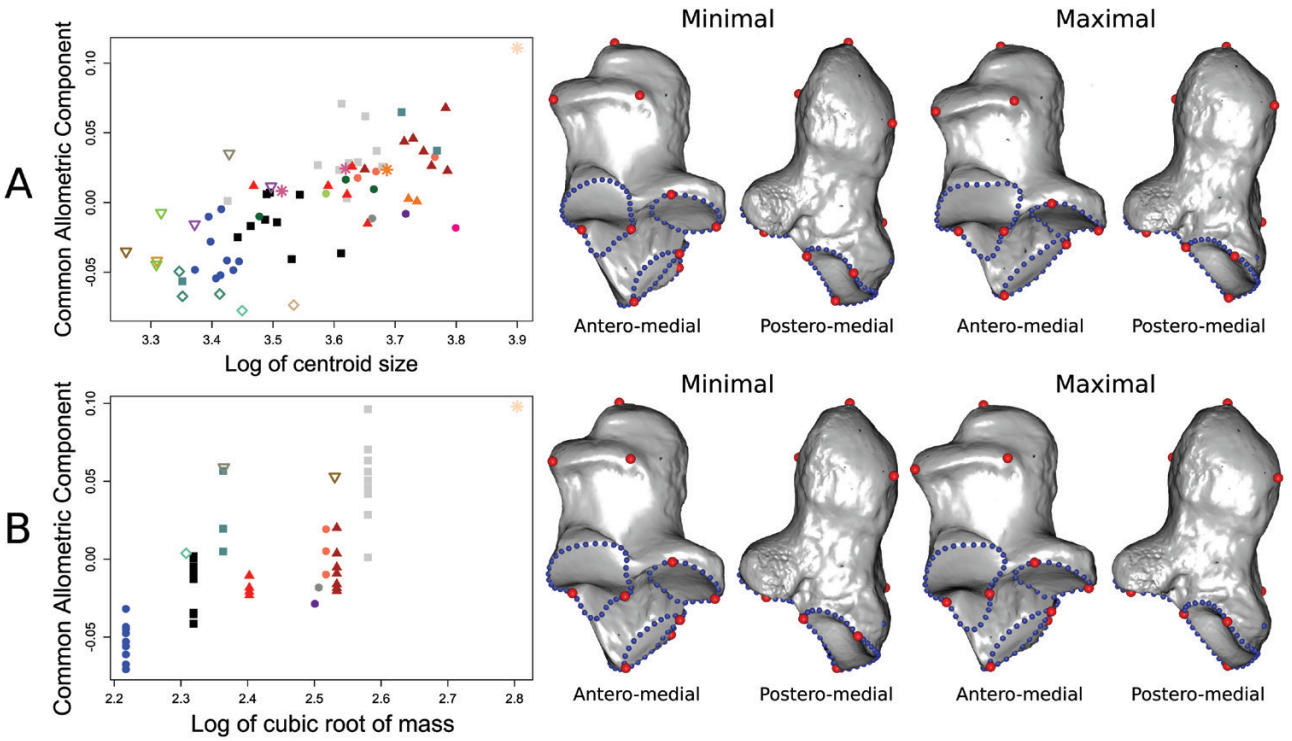

Figure 9. A, regression of the common allometric component on the logarithm of centroid size, with representations of the shapes corresponding to the theoretical maximum and minimum of allometry, on Rhinocerotidae calcanei. B, regression of the common allometric component of allometry-free shapes, on the logarithm of the cubic root of the mean mass of the species, with representations of the shapes corresponding to the theoretical maximum and minimum of mass, on Rhinocerotidae calcanei. Legend as in Figure 8. Vector representations are available in Appendix S7D.

species; the proximal facet for the astragalus is more triangular, and slightly extended medially; the distal facet for the astragalus is extended distally; and the facet for the cuboid is piriform, and wider proximally.

Perissodactyla

Astragalus

The neighbour-joining tree based on astragalar morphology (Fig. 10) shows a relative clustering of the families, with some exceptions. *Moropus* is not grouped with the other chalicotheres but is closer in morphology to the Rhinocerotidae, although it has a long branch, which indicates a particular morphology. *Kalobatippus*, a three-toed anchitheriine equid from the Oligocene, has a morphology closer to tapirs and rhinocerotids than to a modern one-toed equinine or hipparionine equid. The Teleoceratina are found relatively close to *Paraceratherium*, and to a lesser extent to the Chalicotheriinae, as compared to other rhinocerotids. *Teleoceras* itself is closest to the Chalicotheriinae, sharing with them an extremely proximo-distally flattened astragalus. Families are not grouped together according to phylogenetic proximity.

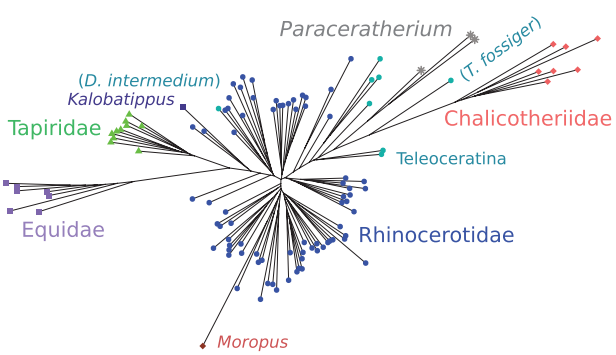

Figure 10. Neighbour-joining tree generated from a matrix of the Euclidian distance between every specimen, on the astragali of Perissodactyla. Extant species are represented as dots and extinct species as squares. Teleoceratina, *Kalobatippus* and *Moropus* belong to Rhinocerotidae, Equidae and Chalicotheriidae, respectively, but are highlighted with regard to their particular positions in the tree. Legend as in Figure 11.

The first three axes of the PCA are presented, as only those axes describe clear shape variations between the families studied, and are correlated with centroid size (PC1 and PC3, negatively: $P < 0.0001$, $R^2 = 0.28$

and $P < 0.001$, $R^2 = 0.19$ respectively; PC2, positively: $P < 0.01$, $R^2 = 0.05$). PC1 and PC3 are more strongly correlated with centroid size than on the analysis with only the Rhinocerotidae, but the R^2value remains well below 50%. The first ten axes explain 77.8% of the variance.

PC1 (37.2% of the variance, Fig. 11) separates five different groups: on the most positive part of the axis are the Equinae. Less positive are the Tapiridae, plus *Kalobatippus*. Around values of 0 are the Rhinocerotidae, except the Teleoceratina, plus *Moropus*. On the negative side are first *Paraceratherium* and the Teleoceratina, our *Teleoceras* specimen having the most negative value among them. The Chalicotheriinae have the most negative values, these being chalicotheres with very short hindlimbs. PC1 is characterized at its negative extremity by a great proximo-distal compression of the bone, twice as wide medio-laterally as high proximo-distally, whereas astragali on the positive end of the axis are approximately equal in width and height. The negative extremity of the axis is also characterized

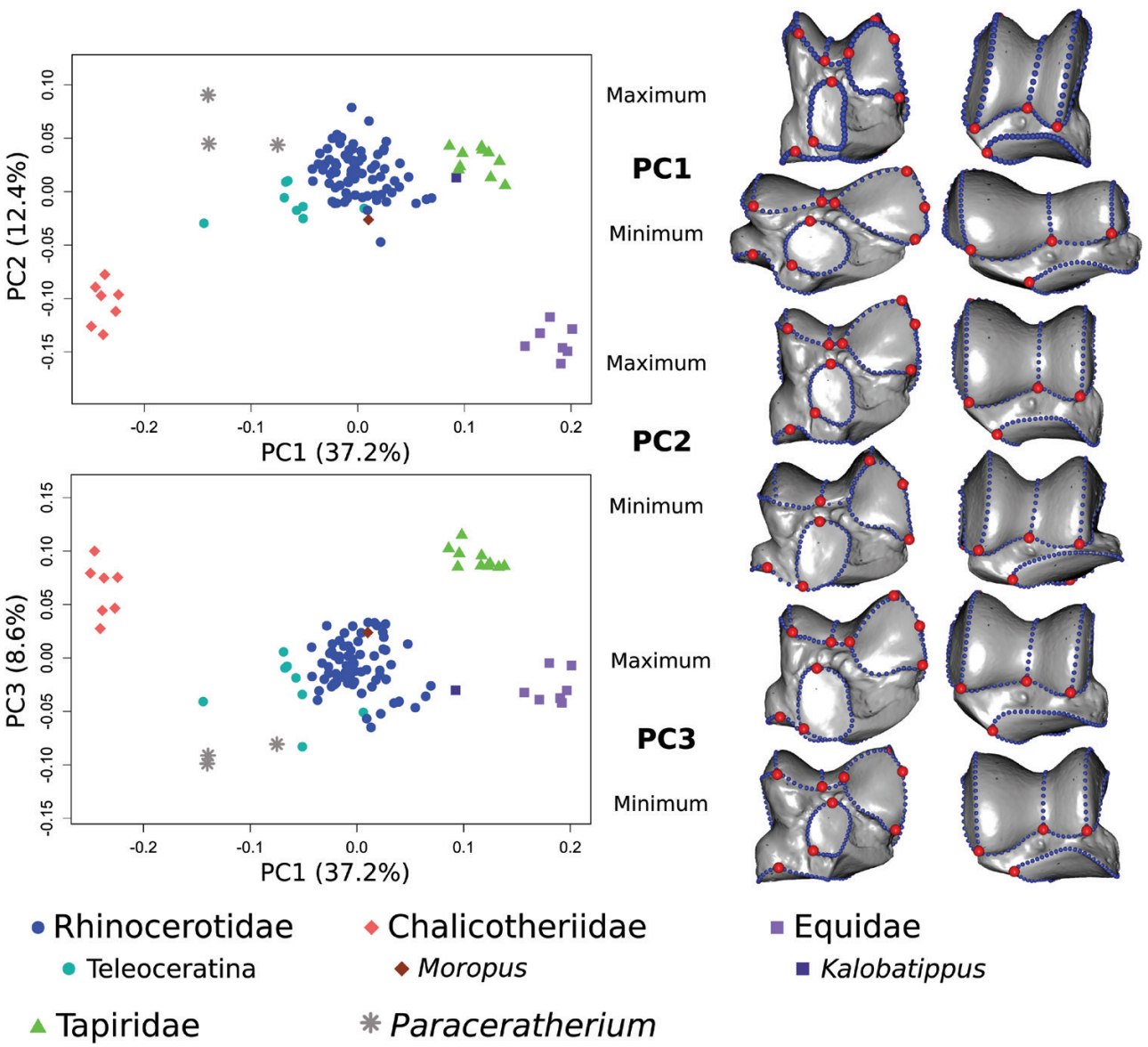

Figure 11. Results of the PCA performed on the astragalus of Perissodactyla. Left: repartition of the Perissodactyla astragali studied across the first three PCA axes. Right: thin-plate-spline deformation of a mean shape towards the maximal and minimal value of each axis. The view is first posterior then anterior. Red dots denote landmarks and blue dots denote curve semi-landmarks. Vector representations of the deformations are provided in Appendix S7E.

by a very flat trochlea with medio-laterally wide, low ridges and a shallow groove, orientated proximally, whereas the trochlea has very high ridges, a very deep groove and is orientated anteriorly on the positive end of the axis; and an extended facet for the fibular malleolus, occupying almost all of the lateral face of the astragalus. Finally, the negative part of PC1 presents a triangular and flat proximal facet for the calcaneus, whereas it is more squared and concave, with a latero-distal extension, on the positive side; a round medial facet for the calcaneus, whereas it is proximo-distally elongated on the positive end of the axis; and an overall wider and flatter facet for the navicular, positioned directly below the body of the astragalus.

PC2 (12.4% of the variance, Fig. 11) separates Equidae (except *Kalobatippus*) and Chalicotheriidae (except *Moropus*) on the negative side from the other families which have more positive values, *Paraceratherium* having the most positive values among them. Astragalar shape variations along PC2 are characterized at the negative extremity by the symmetry of the trochlea, each ridge being of similar height and width whereas the lateral ridge is relatively much wider on the positive end of the axis; the deeper groove of the trochlea; and the greater angular extent of the trochlea. The negative part of PC2 is also characterized by the round shape of the proximal facet for the calcaneus, with a latero-distal extension, whereas it is more square-shaped on the positive end of the axis; the wider medial facet for the calcaneus, positioned very distally, on the edge of the posterior face; the concavity of the lateral contour of the facet for the navicular; the great flatness of the facet for the navicular, whereas it is antero-posteriorly convex on the positive end of the axis; and its position medially offset from the centre of the bone.

On PC3 (8.6% of the variance, Fig. 11) are spread, roughly, from negative values to positive values, *Paraceratherium*, the Rhinocerotidae and Equidae, the Chalicotheriidae, and the Tapiridae, although there is generally an overlap between groups. It is characterized at its negative extremity by a slightly less symmetrical trochlea, with a wider and lower lateral ridge; a distally extended lateral ridge of the trochlea; and a smaller facet for the fibular malleolus, occupying a smaller part of the lateral face of the bone than it does on the positive end of the axis. The negative section of PC3 morphospace is also characterized by a latero-distally extended proximal facet, and a smaller medial facet for the calcaneus, which is positioned more proximally. By comparison, bones at the positive end of PC3 possess medial facets which border the distal side of the posterior face.

Impact of allometry and mass: The centroid size of the astragalus has a significant effect on its shape ($P < 0.001$ and $R^2 = 0.14$ for the astragalus, multivariate regression). A large astragalus (Fig. 12A) is characterized by an overall flat bone, twice as wide medio-laterally as high proximo-distally; medio-laterally wide and low trochlear ridges; a trochlea orientated proximally; a medio-laterally wide and triangle-shaped proximal facet for the calcaneus; a round-shaped medial facet for the calcaneus; and a wide facet for the navicular, which is flat overall and positioned below the body of the astragalus. A small astragalus is as wide as it is high, has higher trochlear ridges and a deeper trochlear groove; a more square-shaped proximal facet for the calcaneus, with a small latero-distal extension; a rectangle-shaped medial facet for the calcaneus, higher proximo-distally than wide medio-laterally; and a smaller facet for the navicular, not directly below the body of the astragalus but medially offset.

Species mass has a statistically significant but very weak effect on allometry-free astragalus shape ($P < 0.05$, $R^2 = 0.027$). An astragalus pertaining to a heavier species (Fig. 12B) has a flatter trochlea with lower ridges; a triangle-shaped proximal facet for the calcaneus; and a medial facet for the calcaneus located more laterally.

Calcaneus

The neighbour-joining tree based on calcaneus morphology (Fig. 13) also shows a relative homogeneity of the families. The closest specimen to the *Paraceratherium* specimen is *Teleoceras fossiger*. Contrary to what was observed for the astragalus, *Moropus* is grouped with the other Chalicotheriidae, although it is not as close to them as they are to each other. Again, families are not grouped following their phylogenetic relationships.

The first two axes are described, as both of them are correlated to centroid size and show clear distinctions between families. PC1 and PC2 are positively correlated with centroid size ($P < 0.001$, $R^2 = 0.27$ and $P < 0.01$, $R^2 = 0.08$, respectively). Again, PC1 is more strongly correlated with regard to size than on the analysis with Rhinocerotidae alone, but the R^2 value remains well below 0.5. The first ten axes explain 79.3% of the variance.

PC1 (31% of the variance, Fig. 14) separates (from the most negative to the most positive values): the Tapiridae, Equidae, Chalicotheriidae, and Rhinocerotidae along with *Paraceratherium*. It is characterized at its negative extremity by a far more elongate and thin tuber calcanei; a relatively smaller proximal facet for the astragalus, reduced proximally, distally and anteriorly; and a smaller facet for the cuboid, narrower because of a postero-lateral reduction.

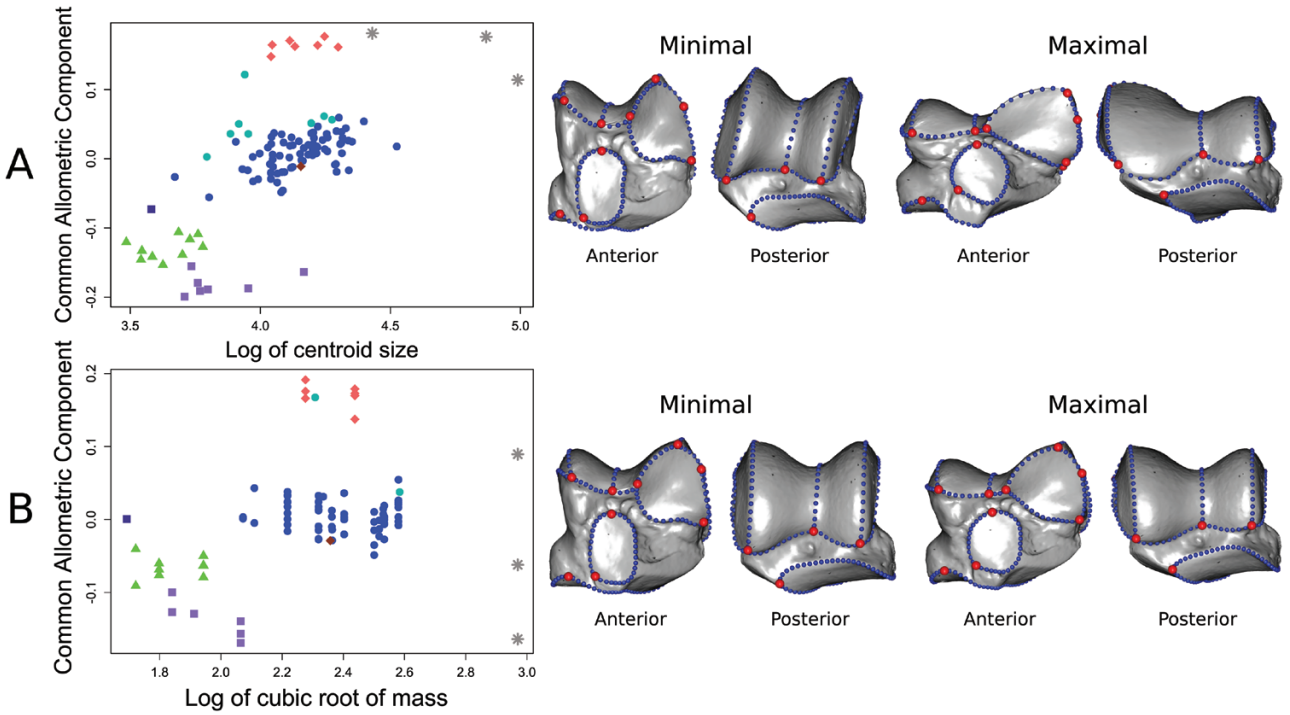

Figure 12. A, regression of the common allometric component on the logarithm of centroid size, with representations of the shapes corresponding to the theoretical maximum and minimum of allometry, on Perissodactyla astragali. B, regression of the common allometric component of allometry-free shapes, on the logarithm of the cubic root of the mean mass of the species, with representations of the shapes corresponding to the theoretical maximum and minimum of mass, on Perissodactyla astragali. Legend as in Figure 11. Vector representations are available in Appendix S7F.

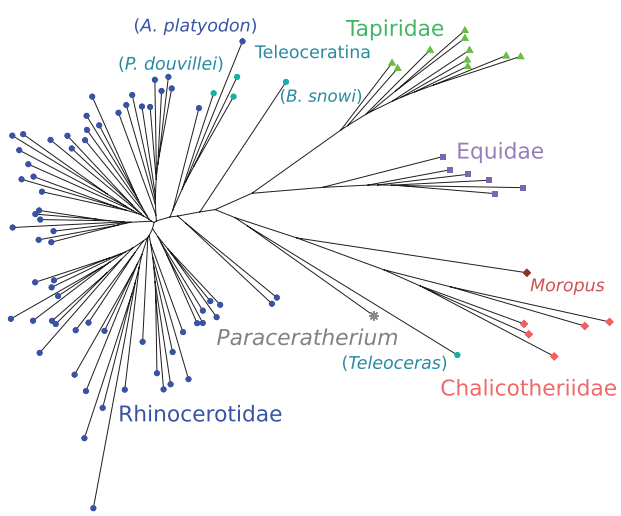

Figure 13. Neighbour-joining tree generated from a matrix of the Euclidian distance between every specimen, on the calcanei of Perissodactyla. Teleoceratina and *Moropus* belong to Rhinocerotidae and Chalicotheriidae, respectively, but are highlighted with regard to their particular positions in the tree. Legend as in Figure 14.

PC2 (16% of the variance, Fig. 14) strongly separates the Chalicotheriidae on the positive side from all the others. Our specimen of *Moropus* has a slightly less positive value than the Chalicotheriinae, and the Tapiridae have more negative values than the Equidae, Rhinocerotidae and *Paraceratherium*. The axis is characterized at its positive extremity by a more elongate and thin tuber calcanei; a head of the calcaneus that is much shorter, accounting for approximately one-third of the total length of the bone whereas on the negative end, it accounts approximately for one-half; a slightly wider, more distally orientated and much more proximally positioned facet for the cuboid, almost in contact with the proximal facet for the astragalus; a proximal facet for the astragalus that is distally very extended; and a wider medial facet for the astragalus, extended medially.

Impact of allometry and mass: The centroid size of the calcaneus has a significant influence on its shape ($P < 0.001$ and $R^2 = 0.11$, multivariate regression). A large calcaneus (Fig. 15A) is characterized by an extreme proximo-distal compression, the

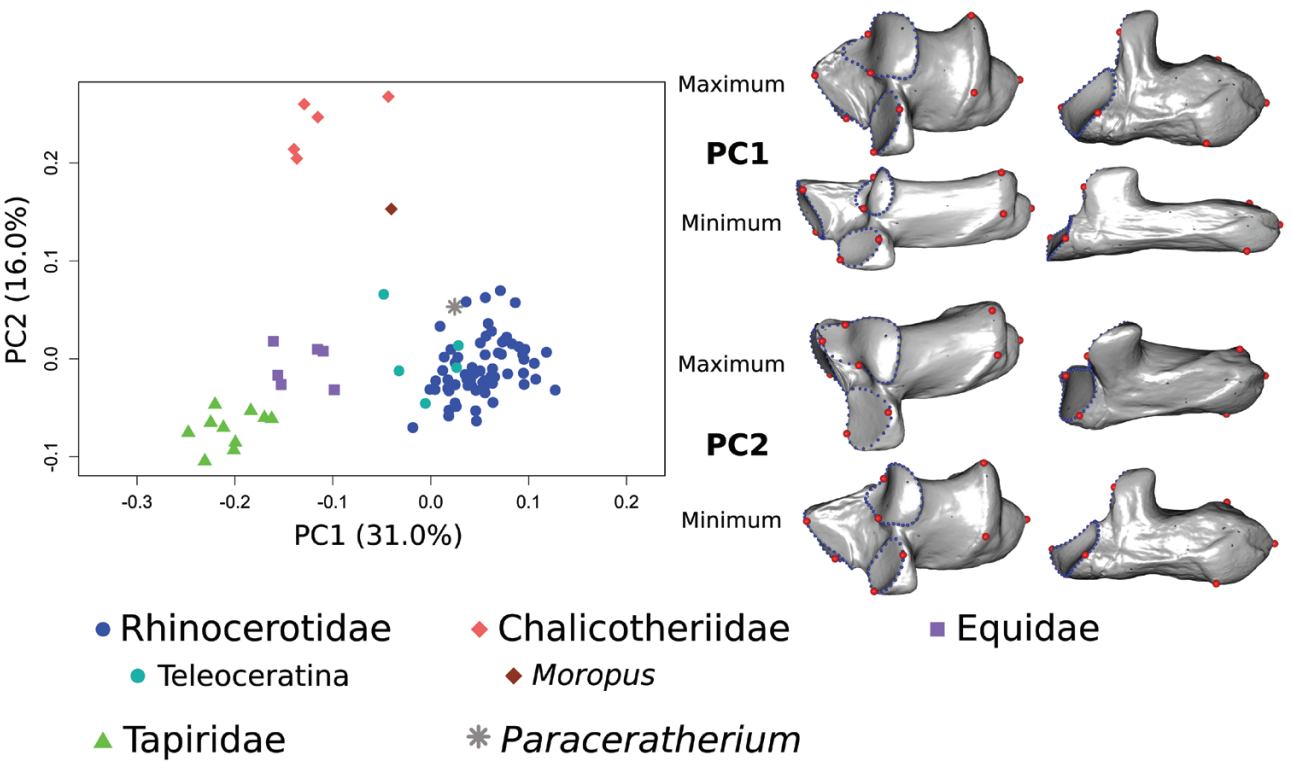

Figure 14. Results of the PCA performed on the calcaneus of Perissodactyla. Left: repartition of the Perissodactyla calcanei studied across the first two PCA axes. Right: thin-plate-spline deformation of a mean shape towards the maximal and minimal value of each axis. The view is first antero-medial then postero-medial. Red dots denote landmarks and blue dots denote curve semi-landmarks. Vector representations of the deformations are provided in Appendix S7G.

tuber calcanei being very robust; a much wider proximal facet for the astragalus, extended in all directions, especially in its proximal half; a distally orientated sustentaculum tali and medial facet for the astragalus; and a wider facet for the cuboid, triangle-shaped and latero-posteriorly extended. A small calcaneus has a very thin tuber calcanei as compared to a large calcaneus; a relatively much smaller overall proximal facet for the astragalus; an anteriorly orientated sustentaculum tali and medial facet for the astragalus; and a relatively smaller facet for the cuboid.

There is a statistically significant influence of species mass on allometry-free calcaneus shape ($P < 0.001$, $R^2 = 0.09$). Shape differences are clear (Fig. 15B), unlike those observed for the same analysis on Rhinocerotidae alone. In our sample, a calcaneus belonging to a heavier species is, on average, characterized by a stouter tuber calcanei; a wider overall proximal facet for the astragalus; a slightly wider medial facet for the astragalus, orientated distally along with the whole sustentaculum tali; and a wider facet for the cuboid, expanding more proximally.

DISCUSSION

First and foremost, it is worth noting that the percentage of variance explained by the first axes of the PCA is usually low (around 66% for the first five axes for the Perissodactyla dataset, 40% for the Rhinocerotidae dataset). The first four or five axes describe the variations between species or families, but the following axes usually distinguish one or two individuals from other specimens of the same taxon. There is indeed great intraspecific variation in the species studied, even if it remains inferior to interspecific variations (Figs 4, 7). For example, *Dicerorhinus sumatrensis* ZSM-1908-571 presents an astragalus with a wide medio-distal extension of the medial facet for the calcaneus, an extension that is absent in all the other specimens. Some specimens of *Ceratotherium simum* present a calcaneus with a fusion of the medial and distal facets for the astragalus, whereas in others they are separated by a deep groove. This could explain the low PC-scores. Indeed, if there are many different variations observed in the sample, these cannot be described on one PC

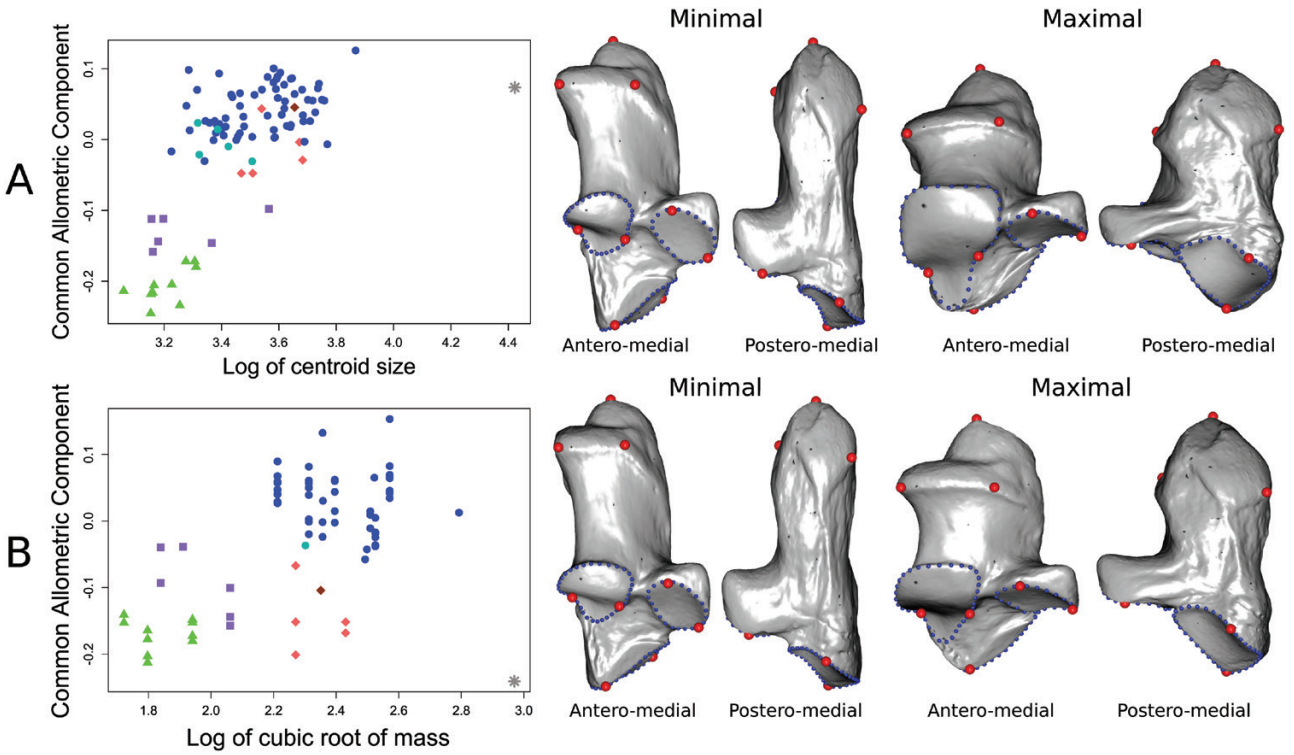

Figure 15. A, regression of the common allometric component on the logarithm of centroid size, with representations of the shape corresponding to the theoretical maximum and minimum of allometry, on Perissodactyla calcanei. B, regression of the common allometric component of allometry-free shapes, on the logarithm of the cubic root of the mean mass of the species, with representations of the shape corresponding to the theoretical maximum and minimum of mass, on Perissodactyla calcanei. Legend as in Figure 14. Vector representations are available in Appendix S7H.

alone and thus the percentage of variation explained by the first axes decreases. On the other hand, if there were a factor clearly driving a continuum of variations in all our sample, we would see a higher percentage of variance for the first axis. That factor is often size (e.g. Bonnan *et al.*, 2013; Cardini *et al.*, 2015; Knigge *et al.*, 2015); here it seems clear that size does not have a strong influence on the shape of the bones, especially in our Rhinocerotidae dataset. We have already noted qualitatively this intraspecific variability between individuals of the same species of Rhinocerotidae when digitizing the bones. It has also been observed by Guérin (1980) on various bones of the tarsus of extant rhinocerotids, by Harrison & Manning (1983) on the carpus bones of *Teleoceras*, and by Heissig (2012) on several limb bones, including the astragalus, of aceratheres. Variations in the age of the specimens, especially for individuals for which we have only an astragalus and no calcaneus or long bones associated, could account for some intraspecific variation. It is difficult to determine the age of individuals using only the astragalus, given that there is no epiphysis on this bone. Additionally, the large number of species, mostly with only one or two individuals, could also result in a greater diversity of morphological variations in our sample and thus lower the variance explained by the first axes. Finally, it appears that Rhinocerotids are a relatively conserved group in terms of the morphology of their astragalus and calcaneus. This could mean that PC scores are driven more by small, individual-specific or species-specific variations than by large-scale variations such as those linked to size or mass.

General influence of mass

The centroid size of both the astragalus and the calcaneus has an effect on their shape (Figs 6, 9). Given that the centroid size of the bone is linked to the mean mass of the species to which it belongs (Supporting Information, Appendix S5), especially on the Perissodactyla dataset, this means that mass has an influence on the shape of the bones in our sample of Perissodactyla. The percentage of variance explained by centroid size or mass, however, is lower than we originally expected. We could indeed expect mass to have a very strong influence on the shape of limb bones, explaining at least 50% of the total variance (Hildebrand *et al.*, 1985; Biewener, 1989; Campione

& Evans, 2012). It appears that, especially when studying only astragali and calcanei of rhinocerotids, which do not vary much in terms of shape, size has no overwhelming influence on the shape of the bone but is instead one factor among others (e.g. possibly habitat, phylogeny and intraspecific variations). Another study on the limb long bones of extant rhinocerotids found a relatively low influence of centroid size on the shape of the bones, although higher than observed here (R^2 between 10 and 18%; Mallet *et al.*, 2019). It is therefore possible that long bones are more affected by size than astragalus and calcaneus.

When centroid size increases, both the astragalus and the calcaneus show an increase in the size of the articular facets. Moreover, in the analysis on Rhinocerotidae alone, the distal and medial facets of each bone for the articulation with the other are fused in specimens with a high centroid size. It could be suggested that wider facets result in a more intricate association between the bones, making the talocalcaneal complex more suited to dissipate compressive forces during limb loading, during plantarflexion or during dorsiflexion of the foot (i.e. flexion or extension of the ankle). In the large astragali belonging to Perissodactyla, the trochlea is orientated proximally, directly facing the tibia and fibula, and has a lower angular extent (Fig. 12). One can assume that this orientation permits complete unfolding of the crurotarsal joint, placing the foot in the same axis as the rest of the limb. This results in a general columnar posture for the limb, as is characteristic of graviportal animals. This columnar posture would help resist twisting, bending and compression forces, and reduce the possibility of dorsiflexion of the autopodium, which would reduce maximal stride length and thus running speed (Hildebrand, 1982). *Paraceratherium* is reported to have had columnar limbs (Osborn, 1923; Prothero, 2013), and our results corroborate this, for the hind autopodium–zeugopodium at least. It can be assumed that the flatter trochlea observed in large astragali, associated with a proximo-distal compression of the bone, fulfils the same role of resistance to twisting and compression. A deeper trochlea would provide more stability for the crurotarsal joint (Polly, 2008), but lead to thinner and therefore more fragile ridges of the trochlea, unable to resist the high forces expected on the ankle of a very heavy animal. This flattening is also observed in Brontotheriidae (Osborn, 1929), Elephantidae (Csuti *et al.*, 2008) and sauropod dinosaurs (Bonnan, 2005), which supports our hypothesis.

For large calcanei belonging to Perissodactyla, beyond the increasing size of the articular surfaces, the main characteristic is that the tuber calcanei is more robust, thicker both medio-laterally and antero-posteriorly, and shorter proximo-distally compared to the total length of the calcaneus (Fig. 15). However, this is only clearly observable when studying our Perissodactyla dataset. The tuber calcanei is a lever arm for the plantarflexion of the foot; two of the muscles inserting on it are responsible for plantarflexion: the gastrocnemius and the soleus (Beddard & Treves, 1889; White & Folkens, 2005). A more robust and shorter tuber would presumably lead to a lower mechanical advantage, requiring a weaker pull from the muscles, which would be easier to resist and reduce bending stress. It could also be a consequence of the proximo-distal shortening of the foot generally observed in heavier species of our sample (Rhinocerotidae, Chalicotheriidae). An animal with an elongated foot would need a longer tuber calcaneus to keep the mechanical advantage constant; conversely, an animal with a short foot would not need a very long lever arm, assuming the mechanical advantage is indeed constant (Biewener, 1989). The correlation of the mean mass of the species on allometry-free shapes of the calcaneus corroborates this result. For two calcanei of the same size but belonging to species of different masses, the one belonging to the heaviest species will have a more robust tuber and wider articular facets (Fig. 15B). This is observable in our analysis in *Ceratotherium simum* and *Rhinoceros unicornis: C. simum* is heavier and has a slightly more robust calcaneus, but on average, the centroid size of its calcaneus is smaller than that of *R. unicornis* (Figs 5, 6). This increased robustness of the body of the calcaneus is found in other mammal families of high body mass (i.e. more than about 2 tons), such as Elephantidae (Chen & Tong, 2017), and also in fossils such as *Pyrotherium* (Shockey & Anaya Daza, 2004). Interestingly, this is not the case in Hippopotamidae, which have a rather elongate calcaneus (e.g. Fisher *et al.*, 2010: figs 6, 8). Hippopotamuses have a body plan close to Teleoceratina, with very short limbs, which also present an elongate calcaneus. Possibly the forces exerted on the calcaneus are less intense for animals with short legs; comparisons with Suidae and Amynodontidae, for example, could yield insights in this regard.

Particular cases linked to body plan and locomotion

As expected, some observed variations in bone shape appear to be linked to the diverse body plans and modes of locomotion of the taxa studied. For the astragalus, equids are characterized by the great depth of their trochlea, a common characteristic in cursorial mammals that provides stabilization of the crurotarsal joint by restricting movement to a parasagittal plan (Polly, 2008). The trochlea is also moderately deep in Rhinocerotidae (except most Teleoceratina) and

Figure 16. Anterior views of the calcanei of *Paraceratherium bugtiense* NHM-PAL-PV-M-100418 (Paraceratheriidae) and *Elasmotherium sibiricum* NHM-PAL-PV-M-12429 (Rhinocerotidae).

Tapiridae, but not in our Chalicotheriinae, animals that probably could not gallop (Coombs, 1983). Teleoceratina specimens also possess very shallow trochleas. Considering their similarity in terms of body plan with hippopotamuses, which cannot gallop (Lewison 2011), it is likely that they could not gallop either, and the shape of their astragalus is consistent with this. *Paraceratherium* and the Chalicotheriinae possess the flattest trochlea of all of our specimens, but still with clearly distinguishable ridges (Figs 11, 12), unlike elephants for instance (e.g. Scarborough *et al.*, 2016). Equids also display a greater angular extent of their trochlea, presumably allowing a greater flexion and extension of the ankle. The most cursorial species (i.e. equids and, to a lower extent, tapirs) possess, on their astragalus, curved facets for the navicular and a curved proximal facet for the calcaneus, whereas those facets are mostly flat in *Paraceratherium* and *Chalicotherium* (Fig. 11). Perhaps the curved facets help to lock the talocalcaneal and talonavicular joints and provide stability for the ankle. The flat facets of heavy species could help to dissipate the forces in the foot homogeneously and facilitate the formation of robust ridges.

A particular shape variation linked to body proportions is the proximo-distal compression of the astragalus across most of our Teleoceratina (Fig. 5). *Diaceratherium* is the only Teleoceratina from our sample having an astragalus similar to that of other rhinocerotids in this regard. Teleoceratina had extremely short, columnar limbs, like modern hippopotamuses. This compression of the astragalus could be linked to the general shortening of the limbs, each segment being proximo-distally shortened, including the basipodium. Interestingly, the astragalus is not compressed in *Diaceratherium intermedium*, a Teleoceratina that is phylogenetically the sister-group to the other Teleoceratina from our sample (Figs 1, 5). It is unclear if *D. intermedium* was short-legged like the other Teleoceratina. The species was placed in the genus *Chilotherium* for a long time, before being reassigned by Antoine *et al.* (2020). Members of the genus *Chilotherium* are characterized by having short legs (Geraads & Spassov, 2009), but no studies have been done specifically on *D. intermedium*. If this species was indeed short-legged, the shortening of the limbs would pre-date the flattening of the astragalus in our sample. The compression of the astragalus does not seem to be dependent on the size of the animal in our Teleoceratina. This condition is observed in both small (e.g. *Prosantorhinus*; <800 kg) and large (*Brachypotherium*; >2000 kg) Teleoceratina (Cerdeño, 1998; Becker, 2003). It is of note that *Paraceratherium* presents the same flattening of the astragalus as our Teleoceratina. Both groups are indeed very close regarding the morphology of their astragalus (Figs 10, 11). *Paraceratherium* is, however, very different from Teleoceratina in that it is very long-legged. It seems that different constraints, i.e. the very high mass of *Paraceratherium* and the short legs and lower mass of Teleoceratina, can produce a similar result in terms of morphology. A study incorporating Amynodontidae (rhinocerotoids with some members, such as *Metamynodon*, being short-legged like Teleoceratina; Wall, 1989), could also yield more insights on this subject. Teleoceratina astragali also differ from those of other rhinocerotids by the distal elongation of their proximal facet with the calcaneus. The facet almost reaches the distal side of the bone, whereas it reaches only halfway in other rhinocerotids (Fig. 5). The facet might need to remain relatively long in order to maintain cohesion between the astragalus and the calcaneus. Thus, when the bone is proximally reduced, the facet retains the same length and occupies relatively more space on the posterior face. *Teleoceras* is an extremely variable genus in terms of bone morphology (Harrison & Manning, 1983), a study with more individuals could thus yield insights on more subtle shape variations.

Chalicotheriinae also present a proximo-distally compressed astragalus. They differ from Teleoceratina and *Paraceratherium* in that their trochlea is orientated more anteriorly, and has a greater angular extent. This seems logical when looking at the angle

of the crurotarsal articulation: the angle is clearly superior to 90°, almost reaching a flat angle, in *Teleoceras* and *Paraceratherium*, giving the limb a columnar posture. However, it is approximatively 90° in *Chalicotherium*, whose hindlimb is far more crouched (e.g. Coombs, 1983: fig. 7B). The extremely flattened astragalus of the Chalicotheriinae is not found in *Moropus*, which shows an astragalus closer to a rhinocerotid. The trochlea in particular is deeper in *Moropus*, whereas it is shallow in *Chalicotherium* and *Anisodon*. The extreme proximo-distal compression of Chalicotheriinae astragali could be a consequence of the reduction in the length of the hind limb, with each part of the limb being reduced, just as in Teleoceratina. This shortening could also be linked to the greater mass carried by shorter hindlimbs, whereas body mass would be more evenly spread on fore- and hindlimbs if they were of equal length. It could also be a consequence of their posture. Chalicotheriinae are indeed described as bipedal browsers. It is assumed that they could adopt an erect posture on their hindlimbs and use their forelimbs to grasp branches and twigs (Zapfe, 1979; Coombs, 1983; Schulz-Kornas *et al.*, 2007). Most of their weight would therefore be supported by the hindlimbs, which would be in accordance with a stronger, flatter astragalus as observed in *Paraceratherium*. *Moropus*, and presumably the Schizotheriinae in general, have hind- and forelimbs of approximately the same length, and were postulated to use bipedal browsing less frequently (Coombs 1982, 1989). This would reduce the advantage of a flatter astragalus. Further studies are needed to confirm or refute these hypotheses, including more individuals belonging to more genera, especially for Schizotheriinae (e.g. *Ancylotherium* or *Metaschizotherium*).

Another bone presenting a shape much different from what would be expected if mass were the single driving factor is the calcaneus of *Paraceratherium*. *Paraceratherium* is by far the heaviest species of our sample, almost twice as heavy as *Elasmotherium* (Table 1). However, its calcaneus is elongated when compared to that of *Elasmotherium*, which has the most robust calcaneus (Figs 15, 16). This could be a consequence of its general body plan: *Paraceratherium* had longer legs than all the rhinocerotids. One might thus suppose that longer legs, and thus a longer autopodium as observed in *Paraceratherium* (Prothero, 2013), would lead to an elongation of the tuber calcanei to keep the mechanical advantage of the lever system of the foot constant. Antoine *et al.* (2004) have indeed observed similarities between the calcaneus of *Paraceratherium* and that of a *Giraffa*. However, Teleoceratina have very short legs and a rather elongated calcaneus as compared to other rhinocerotids (Fig. 6), and elephants have long legs but a very short calcaneus. Other individuals of *Paraceratherium* and *Elasmotherium* are needed to confirm these results, as well as smaller members of the family Paraceratheriidae (e.g. *Pappaceras* and *Juxia*; Wang, 2016). A study including other families of Rhinocerotoidea, such as the small cursorial Hyracondontidae and the short-legged Amynodontidae could provide a better understanding of the question. Ultimately, comparing heavy and stocky mammals, such as *Mixotoxodon* (Notoungulata, Meridiungulata) or *Hippopotamus amphibus* (Hippopotamidae), with heavy and slender mammals, such as *Titanotylopus* (Camelidae) or *Giraffa camelopardalis* (Giraffidae), could also help understand the adaptations in the basipodium of *Paraceratherium*. However, in these extremely disparate taxa, one must be aware of a phylogenetical signal that could mask the changes of shape linked to mass. It is unclear what gait *Paraceratherium* was capable of adopting besides walking. Paul & Christiansen (2000) have suggested it could at least attain a trot. The fact that their astragalus retains clear ridges and that their calcaneus is quite elongated, characteristics reminiscent of cursorial animals (Polly, 2008; Bassarova *et al.*, 2009), is consistent with this suggestion. Elephants possess a completely flat trochlea and a short calcaneus, and are incapable of trotting or galloping.

CONCLUSION

Overall, it appears that mass has an influence on the shape of the astragalus and calcaneus in Rhinocerotidae and in our sample of Perissodactyla. However, that influence is lower than we initially thought, especially among Rhinocerotidae alone. This suggests that Rhinocerotidae is a relatively conserved group in terms of the morphology of those bones, and that other factors, such as phylogeny or intraspecific variations, have more influence. An ecomorphological study could help to determine if habitat could have a role, but would require reliable habitat assignations for the fossil species. Nonetheless, bones belonging to heavier Rhinocerotidae present larger articular facets, presumably to help better dissipate the larger forces involved in the locomotion of heavier animals. The calcaneus is also more robust. In our sample of Perissodactyla, a stronger influence of mass is noted, with again heavier facets and stronger bones overall. We observe a flattened trochlea of the astragalus that would limit the risk of breaking, as compared to lighter animals which have a deeper trochlea with thin ridges providing stability of the crurotarsal joint. Although these features can thus be explained morphofunctionally, the phylogenetic signal is significant and could also explain variations between the families. A larger study encompassing large and

small species of Perissodactyla will be necessary to determine more specifically what drives the shape of these bones in this order. Moreover, comparisons between rhinocerotids and other perissodactyls reveal that body plan has a clear influence on the shape of the bones. Short-legged Teleoceratina display a flattened astragalus and an elongate calcaneus. Chalicotheres with short hindlimbs also display a flattened astragalus compared to chalicotheres with hindlimbs as long as their forelimbs, perhaps linked to the increased mass supported by the hindlimbs. Finally, *Paraceratherium*, which is extremely heavy and relatively long-legged compared to other rhinocerotoids, displays a flat astragalus as expected but a relatively elongate tuber calcaneus, perhaps linked to either its elongate metapodials or its phylogenetic history.

ACKNOWLEDGMENTS

This work acknowledges funding by the European Research Council and is part of the GRAVIBONE project (ERC-2016-STG-715300) allocated to A. H. We acknowledge the very helpful comments of the three reviewers, P.-O. Antoine of the University of Montpellier, J. MacLaren of the University of Liège and M. Mihlbachler of the New York Institute of Technology, and we also would like to thank J. A. Allen of the University of Southampton for editorial work. We thank the curators of all the collections where we digitized specimens: J. Lesur, C. Bens, A. Verguin and G. Billet (Muséum National d'Histoire Naturelle, Paris, France), E. Robert (Université Claude Bernard, Lyon, France), Y. Laurent (Muséum d'Histoire Naturelle de Toulouse, Toulouse, France), C. West, R. Jennings and M. Cobb (Powell-Cotton Museum, Birchington-on-Sea, UK), P. Brewer, R. Pappa and R. Portela Miguez (Natural History Museum, London, UK), A. H. van Heteren (Zoologische Staatssammlung München, Munich, Germany), G. Rößner (Bayerische Staatssammlung fur Palaöntologie und historiche Geologie, Munich, Germany), and F. Zachos, A. Bibl and U. Göhlich (Naturhistorisches Museum, Vienna, Austria).

REFERENCES

3D Systems. 2017. *Geomagic wrap*. Rock Hill: 3D Systems.

Adams DC. 2014. A generalized K statistic for estimating phylogenetic signal from shape and other high-dimensional multivariate data. *Systematic Biology* **63:** 685–697.

Agisoft LLC. 2017. *Agisoft PhotoScan Professional*. St Petersburg: Agisoft.

Alexander R. 1985. Body support, scaling, and allometry. In: Hildebrand M, Bramble DM, Liem KF, Wake D, eds. *Functional vertebrate morphology*. Cambridge: Belknap Press of Harvard University Press, 26–37.

Antoine PO. 1997. *Aegyrcitherium beonensis*, nouvel élasmothère (Mammalia, Perissodactyla) du gisement miocène (MN 4b) de Montréal-du-Gers (Gers, France). Position phylogénétique au sein des Elasmotheriini. *Neues Jahrbuch für Geologie und Paläontologie – Abhandlungen* **204:** 399–414.

Antoine PO. 2002. Phylogénie et évolution des Elasmotheriina (Mammalia, Rhinocerotidae). *Mémoires du Muséum national d'Histoire naturelle* **188:** 1–359.

Antoine PO. 2020. Rhinocerotids from the Siwalik faunal sequence. In: Badgley C, Pilbeam D, Morgan M, eds. *At the foot of the Himalayas: paleontology and ecosystem dynamics of the Siwalik record of Pakistan*. Baltimore: Johns Hopkins University Press (in press).

Antoine PO, Downing KF, Crochet JY, Duranthon F, Flynn LJ, Marivaux L, Métais G, Rajpar AR, Roohi G. 2010. A revision of *Aceratherium blanfordi* Lydekker, 1884 (Mammalia: Rhinocerotidae) from the Early Miocene of Pakistan: postcranials as a key. *Zoological Journal of the Linnean Society* **160:** 139–194.

Antoine PO, Shah SMI, Cheema IU, Crochet JY, De Franceschi D, Marivaux L, Métais G, Welcomme JL. 2004. New remains of the baluchithere *Paraceratherium bugtiense* (Pilgrim, 1910) from the Late/latest Oligocene of the Bugti hills, Balochistan, Pakistan. *Journal of Asian Earth Sciences* **24:** 71–77.

Artec 3D. 2018. *Artec Studio Professional*. Luxembourg: Artec 3D.

Barr WA. 2014. Functional morphology of the bovid astragalus in relation to habitat: controlling phylogenetic signal in ecomorphology. *Journal of Morphology* **275:** 1201–1216.

Bassarova M, Janis CM, Archer M. 2009. The calcaneum—on the heels of marsupial locomotion. *Journal of Mammalian Evolution* **16:** 1–23.

Becker D. 2003. *Paléoécologie et paléoclimats de la Molasse du Jura (Oligo-Miocène): apport des Rhinocerotoidea (Mammalia) et des minéraux argileux*. Doctoral dissertation, Université de Fribourg.

Beddard FE, Treves F. 1889. On the anatomy of *Rhinoceros sumatrensis*. *Proceedings of the Zoological Society of London* **57:** 7–25.

Biewener A. 1989. Mammalian terrestrial locomotion and size. *BioScience* **39:** 776–783.

Biewener A. 1990. Biomechanics of mammalian terrestrial locomotion. *Science* **250:** 1097–1103.

Biewener A, Patek S. 2018. Physical and biological properties and principles. In: Biewener A, Patek S, eds. *Animal locomotion*. New York: Oxford University Press, 1–11.

Blomberg SP, Garland T, Ives AR. 2003. Testing for phylogenetic signal in comparative data: behavioral traits are more labile. *Evolution; International Journal of Organic Evolution* **57:** 717–745.

Bongianni M. 1988. *Simon & Schuster's guide to horses and ponies*. New York: Fireside.

Bonnan MF. 2005. Pes anatomy in sauropod dinosaurs: implications for functional morphology, evolution, and

phylogeny. In: Tidwell V, Carpenter K, eds. *Thunder-lizards: the sauropodomorph dinosaurs*. Bloomington: Indiana University Press, 346–380.

Bonnan MF, **Wilhite DR**, **Masters SL**, **Yates AM**, **Gardner CK**, **Aguiar A. 2013.** What lies beneath: subarticular long bone shape scaling in eutherian mammals and saurischian dinosaurs suggests different locomotor adaptations for gigantism. *PLoS One* **8:** e75216.

Bookstein FL. 1991. *Morphometric tools for landmark data: geometry and biology*. Cambridge: Cambridge University Press.

Botton-Divet L, **Cornette R**, **Fabre AC**, **Herrel A**, **Houssaye A. 2016.** Morphological analysis of long bones in semi-aquatic mustelids and their terrestrial relatives. *Integrative and Comparative Biology* **56:** 1298–1309.

Campione NE, **Evans DC. 2012.** A universal scaling relationship between body mass and proximal limb bone dimensions in quadrupedal terrestrial tetrapods. *BMC Biology* **10:** 60.

Cardini A, **Polly D**, **Dawson R**, **Milne N. 2015.** Why the long face? Kangaroos and wallabies follow the same 'rule' of cranial evolutionary allometry (CREA) as placentals. *Evolutionary Biology* **42:** 169–176.

Carrano MT. 1997. Morphological indicators of foot posture in mammals: a statistical and biomechanical analysis. *Zoological Journal of the Linnean Society* **121:** 77–104.

Cerdeño E. 1998. Diversity and evolutionary trends of the family Rhinocerotidae (Perissodactyla). *Palaeogeography, Palaeoclimatology, Palaeoecology* **141:** 13–34.

Chen X, **Tong H. 2017.** On the hindfoot bones of *Mammuthus trogontherii* from Shanshenmiaozui in Nihewan Basin, China. *Quaternary International* **445:** 50–59.

Cignoni P, **Callieri M**, **Corsini M**, **Dellepiane M**, **Ganovelli F**, **Ranzuglia G. 2008.** MeshLab: an open-source mesh processing tool. In: Proceedings of the 2008 Eurographics Italian Chapter Conference, Salerno, Italy, 129–136.

Coombs MC. 1982. Chalicotheres (Perissodactyla) as large terrestrial mammals. *Third North American Paleontological Convention, Proceedings* **I:** 99–103.

Coombs MC. 1983. Large mammalian clawed herbivores: a comparative study. *Transactions of the American Philosophical Society* **73:** 1–96.

Coombs MC. 1989. Interrelationships and diversity in the Chalicotheriidae. In: Prothero DR, Schoch RM, eds. *The evolution of perissodactyls*. New York: Oxford University Press, 321–340.

Costeur L. 2004. Cenogram analysis of the Rudabánya mammalian community: palaeoenvironmental interpretations. *Palaeontographia Italica* **90:** 303.

Csuti B, **Sargent EL**, **Bechert US. 2008.** *The elephant's foot: prevention and care of foot conditions in captive Asian and African elephants*. Ames: John Wiley & Sons.

Curran SC. 2012. Expanding ecomorphological methods: geometric morphometric analysis of Cervidae post-crania. *Journal of Archaeological Science* **39:** 1172–1182.

Dagosto M, **Terranova CJ. 1992.** Estimating the body size of Eocene primates: a comparison of results from dental and postcranial variables. *International Journal of Primatology* **13:** 307.

Damuth J. 1990. Problems in estimating body masses of archaic ungulates using dental measurements. In: Damuth J, MacFadden BJ, eds. *Body size in mammalian paleobiology: estimation and biological implications*. Cambridge: Cambridge University Press, 229–254.

DeGusta D, **Vrba E. 2003.** A method for inferring paleohabitats from the functional morphology of bovid astragali. *Journal of Archaeological Science* **30:** 1009–1022.

Dinerstein E. 2011. Family Rhinocerotidae (Rhinoceroses). In: Wilson DE, Mittermeier RA, eds. *Handbook of the mammals of the world*. Barcelona: Lynx Edicions, 144–181.

Evin A, **Horáček I**, **Hulva P. 2011.** Phenotypic diversification and island evolution of pipistrelle bats (*Pipistrellus pipistrellus* group) in the Mediterranean region inferred from geometric morphometrics and molecular phylogenetics. *Journal of Biogeography* **38:** 2091–2105.

Fisher RE, **Scott KM**, **Adrian B. 2010.** Hind limb myology of the common hippopotamus, *Hippopotamus amphibius* (Artiodactyla: Hippopotamidae). *Zoological Journal of the Linnean Society* **158:** 661–682.

Fortelius M, **Kappelman J. 1993.** The largest land mammal ever imagined. *Zoological Journal of the Linnean Society* **108:** 85–101.

Gardezi T, **da Silva J. 1999.** Diversity in relation to body size in mammals: a comparative study. *The American Naturalist* **153:** 110–123.

Gaudry M. 2017. *Molecular phylogenetics of the rhinoceros clade and evolution of UCP1 transcriptional regulatory elements across the mammalian phylogeny*. Unpublished D. Phil. Thesis, Univeristy of Manitoba.

Geraads D, **McCrossin M**, **Benefit B. 2012.** A new rhinoceros, *Victoriaceros kenyensis* gen. et sp. nov., and other Perissodactyla from the middle Miocene of Maboko, Kenya. *Journal of Mammalian Evolution* **19:** 57–75.

Geraads D, **Spassov N. 2009.** Rhinocerotidae (Mammalia) from the late Miocene of Bulgaria. *Palaeontographica Abteilung A* **287:** 99–122.

Gladman JT, **Boyer DM**, **Simons EL**, **Seiffert ER. 2013.** A calcaneus attributable to the primitive late Eocene anthropoid *Proteopithecus sylviae*: phenetic affinities and phylogenetic implications. *American Journal of Physical Anthropology* **151:** 372–397.

Gray JE. 1821. On the natural arrangement of vertebrose animals. *London Medical Repository* **15:** 296–310.

Guérin C. 1980. Les rhinocéros (Mammalia, Perissodactyla) du Miocène terminal au Pléistocène supérieur en Europe occidentale: comparaison avec les espèces actuelles. *Documents du Laboratoire de Géologie de la Faculté des Sciences de Lyon* **79:** 1–1182.

Guérin C. 2012. *Anisodon grande* (Perissodactyla, Chalicotheriidae) de Sansan. *Mémoires du Muséum national d'Histoire naturelle* **203:** 279–315.

Gunz P, **Mitteroecker P. 2013.** Semilandmarks: a method for quantifying curves and surfaces. *Hystrix, the Italian Journal of Mammalogy* **24:** 103–109.

Gunz P, **Mitteroecker P**, **Bookstein FL. 2005.** Semilandmarks in three dimensions. In: Slice D, ed. *Modern morphometrics in physical anthropology*. Boston: Springer, 73–98.

Harrison JA, **Manning EM. 1983.** Extreme carpal variability in *Teleoceras* (Rhinocerotidae, Mammalia). *Journal of Vertebrate Paleontology* **3:** 58–64.

Heissig K. 2012. Les Rhinocerotidae (Perissodactyla) de Sansan. *Mémoires du Muséum national d'Histoire naturelle* **203:** 279–315.

Hildebrand M. 1982. *Analysis of vertebrate structure*. New York: Wiley.

Hildebrand M, **Bramble DM**, **Liem KF**, **Wake D. 1985.** *Functional vertebrate morphology*. Cambridge: Belknap Press of Harvard University Press.

Holbrook LT, **Lapergola J. 2011.** A new genus of perissodactyl (Mammalia) from the Bridgerian of Wyoming, with comments on basal perissodactyl phylogeny. *Journal of Vertebrate Paleontology* **31:** 895–901.

Houssaye A, **Fernandez V**, **Billet G. 2016.** Hyperspecialization in some South American endemic ungulates revealed by long bone microstructure. *Journal of Mammalian Evolution* **23:** 221–235.

Jams CM, **Gordon IJ**, **Illius AW. 1994.** Modelling equid/ruminant competition in the fossil record. *Historical Biology* **8:** 15–29.

Klingenberg CP. 1996. Multivariate allometry. In: Marcus LF, Corti M, Loy A, Naylor GJP, Slice DE, eds. *Advances in morphometrics*. Boston: Springer, 23–49.

Klingenberg CP. 2016. Size, shape, and form: concepts of allometry in geometric morphometrics. *Development Genes and Evolution* **226:** 113–137.

Knigge RP, **Tocheri MW**, **Orr CM**, **McNulty KP. 2015.** Three-dimensional geometric morphometric analysis of talar morphology in extant gorilla taxa from highland and lowland habitats. *The Anatomical Record Advances in Integrative Anatomy and Evolutionary Biology* **298:** 277–290.

Lewison RL. 2011. Family Hippopotamidae (Hippopotamuses). In: Wilson DE, Mittermeier RA, eds. *Handbook of the mammals of the world*. Barcelona: Lynx Edicions, 308–319.

MacFadden BJ. 2006. North American Miocene land mammals from Panama. *Journal of Vertebrate Paleontology* **26:** 720–734.

Mallet C, **Cornette R**, **Billet G**, **Houssaye A. 2019.** Interspecific variation in the limb long bones among modern rhinoceroses—extent and drivers. *PeerJ* **7**:e7647.

Martinez JN, **Sudre J. 1995.** The astragalus of Paleogene artiodactyls: comparative morphology, variability and prediction of body mass. *Lethaia* **28:** 197–209.

Medici EP. 2011. Family Tapiridae (Tapirs). In: Wilson DE, Mittermeier RA, eds. *Handbook of the mammals of the world*. Barcelona: Lynx Edicions, 182–203.

Missiaen P, **Smith T**, **Guo DY**, **Bloch JI**, **Gingerich PD. 2006.** Asian gliriform origin for arctostylopid mammals. *Naturwissenschaften* **93:** 407–411.

Mitteroecker P, **Gunz P. 2009.** Advances in geometric morphometrics. *Evolutionary Biology* **36:** 235–247.

Mitteroecker P, **Gunz P**, **Windhager S**, **Schaefer K. 2013.** A brief review of shape, form, and allometry in geometric morphometrics, with applications to human facial morphology. *Hystrix, the Italian Journal of Mammalogy* **24:** 59–66.

Mörs T. 2002. Biostratigraphy and paleoecology of continental Tertiary vertebrate faunas in the Lower Rhine Embayment (NW-Germany). *Netherlands Journal of Geosciences* **81:** 177–183.

Nakatsukasa M, **Takai M**, **Setoguchi T. 1997.** Functional morphology of the postcranium and locomotor behavior of *Neosaimiri fieldsi*, a Saimiri-like Middle Miocene platyrrhine. *American Journal of Physical Anthropology* **102:** 515–544.

Osborn HF. 1923. *Baluchitherium grangeri*, a giant hornless rhinoceros from Mongolia. *American Museum Novitates* **78**.

Osborn HF. 1929. *The Titanotheres of ancient Wyoming, Dakota, and Nebraska*. Washington: Government Printing Office.

Owen R. 1848. Description of teeth and portions of jaws of two extinct Anthracotherioid quadrupeds (*Hyopotamus vectianus* and *Hyop. bovinus*) discovered by the Marchioness of Hastings in the Eocene deposits on the N.W. coast of the Isle of Wight: with an attempt to develop Cuvier's idea of the classification of pachyderms by the number of their toes. *Quarterly Journal of the Geological Society of London* **4:** 103–141.

Panciroli E, **Janis C**, **Stockdale M**, **Martín-Serra A. 2017.** Correlates between calcaneal morphology and locomotion in extant and extinct carnivorous mammals. *Journal of Morphology* **278:** 1333–1353.

Paul GS, **Christiansen P. 2000.** Forelimb posture in neoceratopsian dinosaurs: implications for gait and locomotion. *Paleobiology* **26:** 450–465.

Perrard A, **Villemant C**, **Carpenter JM**, **Baylac M. 2012.** Differences in caste dimorphism among three hornet species (Hymenoptera: Vespidae): forewing size, shape and allometry. *Journal of Evolutionary Biology* **25:** 1389–1398.

Piras P, **Maiorino L**, **Raia P**, **Marcolini F**, **Salvi D**, **Vignoli L**, **Kotsakis T. 2010.** Functional and phylogenetic constraints in Rhinocerotinae craniodental morphology. *Evolutionary Ecology Research* **12:** 897–928.

Plummer TW, **Bishop LC**, **Hertel F. 2008.** Habitat preference of extant African bovids based on astragalus morphology: operationalizing ecomorphology for palaeoenvironmental reconstruction. *Journal of Archaeological Science* **35:** 3016–3027.

Polly D. 2008. Limbs in mammalian evolution. In: Hall BK, ed. *Fins into limbs: evolution, development, and transformation.* Chicago: University of Chicago Press, 245–268.

Prothero DR. 2005. Biogeography and diversity patterns. In: *The evolution of North American rhinoceroses.* Cambridge: Cambridge University Press, 182–199.

Prothero DR. 2013. *Rhinoceros giants: the paleobiology of indricotheres*. Bloomington: Indiana University Press.

Prothero DR, **Guérin C**, **Manning E. 1989.** The history of the Rhinocerotoidea. In: Prothero DR, Schoch RM, eds. *The evolution of perissodactyls*. New York: Oxford University Press, 321–340.

Prothero DR**,** Schoch RM, **eds**. **1989.** *The evolution of perissodactyls*. New York: Oxford University Press.

R Development Core Team. **2005.** *R: a language and environment for statistical computing*. Vienna: R Foundation for Statistical Computing.

RStudio, Inc. **2018.** *RStudio*. Boston: RStudio, Inc.

Rubenstein DI. 2011. Family Equidae (Horses and relatives). In: Wilson DE, Mittermeier RA, eds. *Handbook of the mammals of the world*. Barcelona: Lynx Edicions, 106–143.

Saarinen J, **Eronen J**, **Fortelius M**, **Seppä H**, **Lister A. 2016.** Patterns of diet and body mass of large ungulates from the Pleistocene of Western Europe, and their relation to vegetation. *Palaeontologia Electronica* **19:** 1–58.

Scarborough ME, **Palombo MR**, **Chinsamy A. 2016.** Insular adaptations in the astragalus–calcaneus of Sicilian and Maltese dwarf elephants. *Quaternary International* **406:** 111–122.

Schlager S, **Jefferis G**, **Dryden I. 2018.** *Morpho: a toolbox providing methods for data-acquisition, visualisation and statistical methods related to Geometric Morphometrics and shape analysis*. Available at: https://rdrr.io/cran/Morpho/man/Morpho-package.html

Schulz-Kornas E, **Fahlke JM**, **Merceron G**, **Kaiser T. 2007.** Feeding ecology of the Chalicotheriidae (Mammalia, Perissodactyla, Ancylopoda). Results from dental micro- and mesowear analyses. *Verhandlungen des Naturwissenschaftlichen Vereins zu Hamburg* **43:** 5–32.

Semprebon GM, **Sise PJ**, **Coombs MC. 2011.** Potential bark and fruit browsing as revealed by stereomicrowear analysis of the peculiar clawed herbivores known as chalicotheres (Perissodactyla, Chalicotherioidea). *Journal of Mammalian Evolution* **18:** 33–55.

Shockey B, **Anaya Daza F. 2004.** *Pyrotherium macfaddeni*, sp nov (Late Oligocene, Bolivia) and the pedal morphology of pyrotheres. *Journal of Vertebrate Paleontology* **24:** 481–488.

Stains HJ. 1959. Use of the calcaneum in studies of taxonomy and food habits. *Journal of Mammalogy* **40:** 392–401.

Steiner CC, **Ryder OA. 2011.** Molecular phylogeny and evolution of the Perissodactyla: phylogeny of the perissodactyls. *Zoological Journal of the Linnean Society* **163:** 1289–1303.

Tsubamoto T. 2014. Estimating body mass from the astragalus in mammals. *Acta Palaeontologica Polonica* **59:** 259–265.

Valli AM. 2005. Taphonomy of the late Miocene mammal locality of Akkasdagı, Turkey. *Geodiversitas* **27:** 793–808.

Wall WP. 1989. The phylogenetic history and adaptive radiation of Amynodontidae. In: Prothero DR, Schoch RM, eds. *The evolution of perissodactyls*. New York: Oxford University Press, 341–354.

Wang H, **Bai B**, **Meng J**, **Wang Y. 2016.** Earliest known unequivocal rhinocerotoid sheds new light on the origin of giant rhinos and phylogeny of early rhinocerotoids. *Scientific Reports* **6:** 39607.

White TD, **Folkens PA. 2005.** Foot: tarsals, metatarsals, & phalanges. In: White TD, Folkens PA, eds. *The human bone manual*. San Diego: Academic Press, 287–308.

Wiley DF. 2005. *Landmark*. Davis: Institute for Data Analysis and Visualization, University of California.

Willerslev E, **Gilbert MTP**, **Binladen J**, **Ho SY**, **Campos PF**, **Ratan A**, **Tomsho LP**, **da Fonseca RR**, **Sher A**, **Kuznetsova TV**, **Nowak-Kemp M**, **Roth TL**, **Miller W**, **Schuster SC. 2009.** Analysis of complete mitochondrial genomes from extinct and extant rhinoceroses reveals lack of phylogenetic resolution. *BMC Evolutionary Biology* **9:** 95.

Zapfe H. 1979. *Chalicotherium grande (BLAINV.) aus der miozänen Spaltenfüllung von Neudorf an der March (Děvinská Nová Ves), Tschechoslowakei*. Vienna, Austria: Berger.

Zhegallo V, **Kalandadze N**, **Shapovalov A**, **Bessudnova Z**, **Noskova N**, **Tesakova E. 2005.** On the fossil rhinoceros *Elasmotherium* (including the collections of the Russian Academy of Sciences). *Cranium* **22:** 17–40.

SUPPORTING INFORMATION

Additional Supporting Information may be found in the online version of this article at the publisher's website.

Appendix S1. List of all the specimens studied.
Appendix S2. Anatomical description of the bones.
Appendix S3. Description of the landmarks and curves placed on the bones.
Appendix S4. Results of the repeatability tests.
Appendix S5. Correlation between centroid size and mean body mass.
Appendix S6. Results of the K-mult test.
Appendix S7. Vector representations of all the shape variations described.
Figure S1. Right astragalus of *Rhinoceros unicornis* MNHN-ZM-AC-1960-59, in A: anterior, B: lateral, C: posterior and D: distal views. LR: lateral ridge of the trochlea, MR: medial ridge of the trochlea, G: groove of the trochlea, Tr: trochlea, F TM: facet for the tibial malleolus, F FM: facet for the fibular malleolus, F N: facet for the navicular, F Cu: facet for the cuboid, PF C: posterior facet for the calcaneus, MF C: medial facet for the calcaneus, DF C: distal facet for the calcaneus, M T: medial tubercle, P T: posterior tubercle.
Figure S2. Right calcaneus of *Ceratotherium simum* MNHN-ZM-MO-2005–297, in A: anterior, B: medial and C: distal views. TUBER: tuber calcanei, HEAD: head of the calcaneus, ST: sustentaculum tali, RC: rostrum calcanei, GA: great apophysis, MF A: medial facet for the astragalus, PF A: proximal facet for the astragalus, DF A: distal facet for the astragalus, F Cu: facet for the cuboid, L T: lateral tubercle.
Figure S3. Results of the PCA with ten replicates of the landmarks on three different but morphologically close individuals, for each bone.

Figure S4. Regression plot of the logarithm of the centroid size of each individual against the logarithm of the cubic root of the mean mass of its species, for both bones and for both the Rhinocerotidae and the Perissodactyla datasets.

Figure S5. A, vector representations of the shape variations on PC1, PC2 and PC4 on the analysis on the astragalus of Rhinocerotidae. Posterior view. B, left: vector representations of the shape corresponding to theoretical minimum and maximum of allometry on the astragalus of Rhinocerotidae. Right: vector representations of the shape corresponding to theoretical minimum and maximum of mass on allometry-free shapes on the astragalus of Rhinocerotidae. Posterior view. C, vector representations of the shape variations on PC1 and PC2 on the analysis on the calcaneus of Rhinocerotidae. Antero-medial view. D, left: vector representations of the shape corresponding to theoretical minimum and maximum of allometry on the calcaneus of Rhinocerotidae. Right: vector representations of the shape corresponding to theoretical minimum and maximum of mass on allometry-free shapes on the calcaneus of Rhinocerotidae. Antero-medial view. E, vector representations of the shape variations on PC1, PC2 and PC3 on the analysis on the astragalus of Perissodactyla. Posterior view. F, left: vector representations of the shape corresponding to theoretical minimum and maximum of allometry on the astragalus of Perissodactyla. Right: vector representations of the shape corresponding to theoretical minimum and maximum of mass on allometry-free shapes on the astragalus of Perissodactyla. Posterior view. G, vector representations of the shape variations on PC1 and PC2 on the analysis on the calcaneus of Perissodactyla. Antero-medial view. H, left: vector representations of the shape corresponding to theoretical minimum and maximum of allometry on the calcaneus of Perissodactyla. Right: vector representations of the shape corresponding to theoretical minimum and maximum of mass on allometry-free shapes on the calcaneus of Perissodactyla. Antero-medial view.